Article

Ultrafast Dynamics and Coherent Oscillations in Ethylene and Ethylene-*d* Excited at 162 nm

K. Kosma, S. A. Trushin, W. Fuss, and W. E. Schmid

J. Phys. Chem. A, **2008**, 112 (33), 7514-7529• DOI: 10.1021/jp803548c • Publication Date (Web): 29 July 2008

Ultrafast Dynamics and Coherent Oscillations in Ethylene and Ethylene-d_4 Excited at 162 nm

K. Kosma, S. A. Trushin, W. Fuss,* and W. E. Schmid

Max-Planck-Institut für Quantenoptik, D-85741 Garching, Germany

Received: April 23, 2008; Revised Manuscript Received: June 9, 2008

The fifth harmonic (162 nm, 11 fs), generated in a short argon cell from 12 fs Ti−sapphire laser pulses, was used to excite C_2H_4 and C_2D_4 in the maximum of the first $\pi\pi^*$ transition. Around 10% of the molecules were excited to the π3s Rydberg state instead. The subsequent motion of the wave packet, moving over the potentials from the Franck−Condon region down to the ground state, was monitored by nonresonant ionization at 810 nm with mass-selective detection of the ion yield. Five time constants (from ≈20 fs in excited states to 0.6−11 ps in the hot ground state) and four coherent oscillations (CC stretch and torsion vibrations or hindered free rotation) were determined for each isotopomer. The initial relaxation follows a superposition of CC twist and stretch coordinates; this explains a surprisingly small deuterium isotope effect of the initial time constant (21 versus 24 fs). Also the vibrations in the Franck−Condon region have such a mixed character and a correspondingly small isotope shift. From the perpendicular minimum the wave packet reaches (within 17 or 21 fs for the two isotopomers) a conical intersection via a direction that also involves partial hydrogen migration. This is concluded from the detection of ethylidene (CH_3CH), formed simultaneously with ground-state ethylene. This carbene isomerizes in the ground state within 0.6 ps (1.6 ps for CD_3CD) to ethylene. Two time constants for dissociation (4.5 and 11 ps) in the hot ground state were also identified. The small yields of bimolecular reactions (photodimerization, addition reactions involving a "suddenly polarized" excited state, carbene reactions) are interpreted in terms of the short lifetimes. It is pointed out that the relaxation path starting from the Rydberg state merges into that from the $\pi\pi^*$ state; nevertheless, there is a wavelength dependence in the photochemistry of olefins, because due to a momentum effect the wave packet remembers from which state it came.

1. Introduction

To a large part, $\pi \rightarrow \pi^*$ excitation is involved in the spectroscopy and photochemistry of organic molecules. The simplest such systems are monoolefins. Ethylene is a prototype of them. Its $\pi \rightarrow \pi^*$ absorption begins very weakly around 200−210 nm, reaching a maximum near 162 nm (7.65 eV), where it is, however, superimposed by a Rydberg transition[1−4] (Figure 1). There is now agreement that the weak and diffuse structure at long wavelengths must be assigned to a CC twist vibration and that the excited state has a minimum at 90° twist.[2,4−6] Experimentally this was established by the deuterium effect on this structure at long wavelengths[7,8] and by the resonance Raman spectrum.[9,10] A CC stretch vibration is also expected to be Franck−Condon active[9−12] and was tentatively assigned to some features in the spectrum of C_2D_4;[8] the composed nature of the vibrational structure and the different D effect on these two vibrations is considered to be the reason the C_2D_4 spectrum looks so different (Figure 1).[8,13] (See, however, ref 14 where the vibrational structure was simulated without CC stretch activity. For previous controversies of assignment of the vibrational structure, see refs 3, 4, and 15.) The extrapolated 0−0 transition (hence, the minimum of the torsional potential) would be around 5.6 eV,[5,8] 2.0 eV below the Franck−Condon region (maximum of the torsional potential). In the nomenclature of Mulliken,[2] the $\pi\pi^*$ state is called V (valence excited) state, whereas N (normal) denotes the ground state.

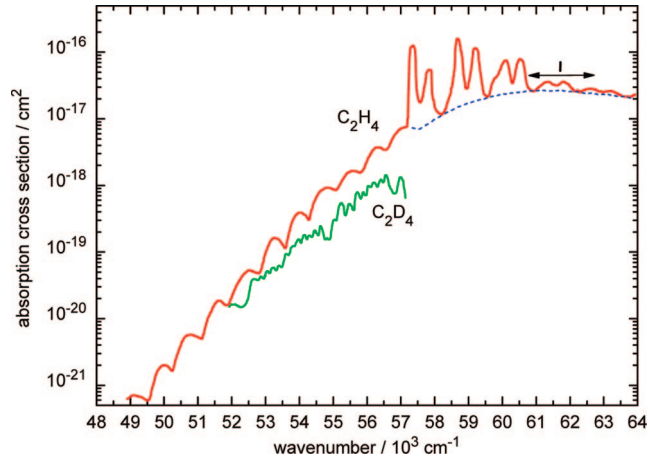

Figure 1. UV spectra of ethylene and ethylene-d_4 (adapted from refs 1 and 2), with the wavelength and bandwidth of the excitation laser also indicated. The dotted line is the estimation of refs 1 and 2 for the $\pi\pi^*$ background below the Rydberg transition. See also the spectra shown in refs 10 and 16.

Quantum chemical calculations of the potential[12,17−21] agree with this picture but add further details: On twisting, a two-electron excited zwitterionic state π^{*2} (Z) crosses the one-electron excited $\pi\pi^*$ state and is slightly below it at 90°.[12,17−21] (The π and π^* orbitals are degenerate at this

* Corresponding author. E-mail: w.fuss@mpq.mpg.de. Fax: +49-89-32905-200.

10.1021/jp803548c CCC: $40.75
Published on Web 07/29/2008

geometry.) This state is easily polarized in polar media ("sudden polarization"[17,22,23] for more recent work, see refs 24 and 25 and literature quoted), leading to a structure with a planar partially positive CH_2 group and a pyramidalized partially negative CH_2 group; the latter group also reduces its HCH angle.[25] Photochemical reactions with polar reagents were therefore expected. Taking also other coordinates into account, the "perpendicular minimum" of the lower state turns out to be a saddle point: the energy is further lowered on pyramidalizing one of the CH_2 groups (already in the absence of polar media)[17−21,26−28] and/or allowing one of the H atoms to partially migrate to the other carbon atom.[12,17,19,20,26,29−32] Along one or both of these coordinates, the molecule can eventually reach a conical intersection (CI) with the ground state. If this path is barrierless (the calculations are not yet reliable enough to decide), it may explain the ultrashort lifetime of the excited state of ethylene. Compared with the measurements (see below), the calculated lifetimes[12,28,33−39] are generally too long, however.

The CI provides not only an ultrafast path for internal conversion but also the branching region between reactant and product formation. Because its geometrical structure involves a 90 °C CC twist, one can expect a high quantum yield of cis−trans isomerization of substituted ethylenes. If it also involves partial H migration (as predicted in refs 12, 19, 20, 26, and 29−32 but questioned in refs 27, 28, 38, and 39), completion of the migration on passing through the CI will give rise to a carbene (in this case ethylidene, CH_3CH). The photochemistry of ethylene and monoolefins has been reviewed.[40−42] Besides cis−trans isomerization, carbene products are observed as a rule.[3,4,40−44] In the case of ethylene itself, an evidence is the formation of methyl-cyclopropane and 1-butene in solid or liquid ethylene,[45] probably formed from a bimolecular insertion of ethylidene into the C=C and C−H bonds of ethylene. It has been suggested,[46,47] and we provide experimental evidence that ethylidene is formed from the same conical intersection as that for cis−trans isomerization and internal conversion. The short-lived ethylidene is detected in this work for the first time.

Other reactions observed after UV excitation of ethylene are the eliminations of atomic and molecular hydrogen (see the reviews on olefin photochemistry[40−42]). The dynamics of these dissociation reactions has been much investigated by photofragment spectroscopy in molecular beams by the group of Y. T. Lee [48−56] and others.[57] There is now agreement that they occur in the hot ground state of ethylene (after internal conversion) or ethylidene.[50−58] In fact, we also observe two ground-state reactions, for the first time in time-resolved work on ethylene and ethylene-d_4.

The dynamics of ethylene was investigated by pump−probe experiments before, but with much less time resolution.[59−62] Probing was done by transient ionization, similarly as in our work. Whereas in the first work[59] the pump wavelength was 155 nm and the time resolution was ≈350 fs, in the other three, ethylene was excited in its long-wavelength wing near 200 nm with pulses of 125−180 fs duration. Probing was done by photoionization mostly at short wavelength (≤267 nm); it allowed determination of only one time constant, the lifetime of population in the Franck−Condon region. Only in the last investigation[62] was a long wavelength (800 nm) also used for ionization (as in most of our work), so that also a second time could be determined. (At longer wavelengths and the required higher intensities, also states of lower electronic energy can be detected, in particular if also ionic fragments are measured.[47,63])

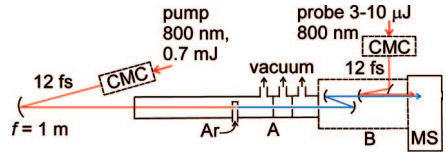

Figure 2. Set-up for the fifth-harmonic generation. The entrance window (CaF_2) is 0.5 mm thick. The probe pulses used for the time-resolved measurements in the time-of-flight mass spectrometer (MS) merge with the UV beam at a mirror with a hole. CMC: chirped-mirror compressor. A is the first of four apertures for differential pumping. B is an evacuated box with mirrors for collimation, focusing and merging the beams.

In this work we use 11−12 fs pulses at 162 nm to pump ethylene in the maximum of its $\pi\pi^*$ band (exciting some molecules also to the π3s Rydberg state, Figure 1) and 12 fs pulses at 810 nm to probe them by (multiphoton) ionization and mass-selective detection of the ion yields; the resulting time resolution is <13 fs. We can resolve five time constants (including two after return to the electronic ground state) and four coherent oscillations (vibrations in the Franck−Condon region and in the perpendicular minimum) for each, C_2H_4 and C_2D_4. These data allow conclusions on the photochemical pathway and provide spectroscopic data not available before.

For the pump pulses we use the fifth harmonic of 12 fs pulses at 810 nm, which themselves are made by self-phase modulation in argon and chirped-mirror compression.[64] The fifth harmonic is produced in an argon cell that is short enough to avoid pulse lengthening;[65] this is an extension of the work, in which 10 fs third-harmonic and supercontinuum pulses were demonstrated.[66]

2. Experimental Section

The generation of short (11 fs) pulses at the fifth harmonic from 12 fs pulses of Ti−sapphire radiation is described in ref 65 and the shortening of the fundamental in ref 67. Briefly, we focused (f = 2 m) 1 mJ pulses (810 nm, 45 fs, 1 kHz) of a commercial Ti−sapphire laser system into a cell (length 1.5 m, equipped with quartz-glass windows of 0.2 mm thickness) filled with 500 mbar Ar (instead of atmospheric-pressure of Ar as in ref 64). Under these conditions the pulses are self-phase modulated and acquire a chirp, which can be used to compress the pulses to 12 fs (determined by a commercial autocorrelator) by reflection from chirped mirrors.[64,67] Part (3−10 μJ) of this radiation was used for probing. The larger part (0.7 mJ) was focused into a short (18 mm) steel cell with two pinholes (0.7 mm), which contained Ar (≈50 mbar) and was immersed in a vacuum setup (Figure 2), where the beam path was differentially pumped. In chamber B the 162 nm radiation was selected by dielectric mirrors and merged with the probe beam, using a mirror with a hole (diameter 4 mm). The two beams were focused (f = 0.7 and 1 m) into the ionization region of a time-of-flight mass spectrometer. With the estimated UV pulse energy of 4 nJ,[65] one calculates an energy density of 0.13 mJ cm^{-2} (intensity 1.3 × 10^{10} W cm^{-2}) in the focus; the intensity of the probe was ≈(3−10) × 10^{13} W cm^{-2}. The pressures of the gases (Xe for determination of the UV pulse duration and the time zero, and ethylene) were between 10^{-7} and 10^{-4} mbar, the latter for the weakest signals.

The signals are the yields of the parent and fragment ions ($C_2H_4^+$, $C_2H_3^+$, $C_2H_2^+$, and the corresponding deuterated species) as functions of the probe delay, which was varied in steps of 3.3 fs. The time zero was taken from the maximum of the Xe^+ signal (from added Xe) recorded in parallel with the other signals, using boxcar integrators. Details on this technique

(time-resolved intense field dissociative ionization) including evaluation can be found in refs 63 and 68 for example.

3. Results

The time-resolved data reflect the population flowing via the different locations L_i on the potential surfaces and the mass spectra ${}^m\sigma_i$ associated with each L_i. In addition, vibrations in L_i can periodically modulate the ${}^m\sigma_i$ (probability to produce an ion of mass m from location i). The populations are modeled by rate equations, whose solutions are sums of exponentials (no matter whether the processes are consecutive or parallel) with time constants τ_i as parameters and coefficients that result from solution of the rate equations. These sums (L_i populations) must still be multiplied by the ${}^m\sigma_i$ (which are another set of fit parameters) to get the signals. To simulate the signal also during the pump−probe overlapping time, these sums of exponentials must be convoluted with the (Gaussian) pump and probe pulses. These procedures are described in detail in refs 63 and 68 If there is in addition a periodic modulation, these functions are multiplied by (one or more) functions of the kind

$$f_{\mathrm{osc}} = 1 + A\cos(2\pi\nu t - \varphi) \qquad (1)$$

where the amplitude A, frequency ν and phase φ are again fit parameters. In practice, one first fits a sum of exponentials (with convolution, if necessary) to the measured signals, then divides the latter by the former and takes the Fourier transform of the result (diminished by 1) to get the frequencies. These are entered into functions of type (1), which are then multiplied by the (convoluted) sum of exponentials; this complete function is then fitted to the measured data to get also the parameters A and φ and a final correction of the time constants τ_i and cross sections ${}^m\sigma_i$. Evaluation in the presence of oscillations is described in more detail in ref 69 Each τ_i and oscillation frequency ν_i in general appear in more than one signal.

It should be noted that, in contrast to previous cases,[69] eq 1 does not contain a dephasing term (exponential decay) before the cosine, because it turned out that all detected oscillations decay with the lifetime of the population at the corresponding location. It seems that there is no opportunity for a dephasing of the oscillations within the short lifetimes.

The evaluation model deserves some further explanation: We assume that on the potential surfaces one can define some contiguous regions (i.e., without gaps, locations L_i). The borders between them result from properties of the probe process, the change of ionization probability and fragmentation pattern. (The fact that this change is continuous might be a reason why the L_i populations obey rate equations, which are normally used for incoherent processes.) The locations have a certain extension, indicated by arrows in the figures. We write the "lifetimes" (of the populations within these extended regions) besides the arrows, if the traveling times of the wave packet through these windows is expected in the same range. Vibrations in these (extended) regions can modulate the ionization and/or fragmentation probability and thus modulate the signal. Hence in this model, it is not the population that oscillates (it is described by a sum of exponentials) but only the signal generation probability.

Figure 3a,b shows the parent ion signals $C_2H_4^+$ and $C_2D_4^+$. Obviously, each exhibits a doubly exponential decay. Because the pump pulse gives rise to two different kinds of excited molecules, some in the $\pi\pi^*$ state and about 10% in the Rydberg state (Figure 1), it seems obvious that the weaker signal (which in fact has an amplitude of ≈10% of the other) with the longer time constant (τ_R = 80 and 115 fs, respectively) belongs to the Rydberg molecules. If the Rydberg state were depleted into a nondetected state, then, to isolate the signal of the $\pi\pi^*$ molecules, one had simply to subtract this monoexponential function (which does not contain any periodic modulation), extrapolated back to time 0 and convoluted with the laser pulses. However, in the Discussion we will show that the Rydberg population flows to the $\pi\pi^*$ state. The signal from this indirect $\pi\pi^*$ population is doubly exponential (time constants τ_R and the lifetime of the $\pi\pi^*$ state, τ_1), with coefficients resulting from the rate equations and the assumption that the ionization probabilities from the two states are equal. This signal part is also subtracted from the measured data (Figure 3a,b); the difference (Figure 3c,d) represents the signal from the directly populated $\pi\pi^*$ state. The result is a singly exponential decay (fit curves in Figure 3c,d, with τ_1 = 21 and 24 fs, respectively) with some modulation. Dividing the data by the (convoluted) exponential fit curve results in the periodic functions at the bottom of Figure 3c,d, whose Fourier transforms are shown separately (Figure 3e,f). The extracted frequencies, time constants and other fit parameters (also for the fragment signals) are compiled in Table 1.

It is easy to show that the two variants of evaluation (subtraction of the, back-extrapolated, slow decay versus subtraction of the full Rydberg path: the Rydberg component decaying with τ_R and the indirect $\pi\pi^*$ population containing τ_R and τ_1) result in the same time constants. (Hence the data do not tell the destination, to where the Rydberg population is depleted.) Only the interpretation of the coefficients is different. However, if there were a highly damped oscillation in the directly populated $\pi\pi^*$ state, it would only be revealed by subtracting the full Rydberg path. Therefore we preferred this method in Figure 3. (An overdamped oscillation was not detected, however.) For the later locations, this method seemed not necessary, so that we simply subtracted the back-extrapolated slow decay in Figure 4.

Figure 4 shows early time data for the fragments $C_2H_2^+$ and $C_2D_2^+$. This stronger earlier part also contains the time constants (τ_1, τ_R) and modulation found already from the parent signal. Obviously the mass spectra of L_1 and L_R also contain these fragment ions. To reveal additional information, we first subtract the slower (τ_R) decay, with the results shown in Figure 4c,d (solid circles). Then we subtract the L_1 contributions, i.e., an exponential with time constant τ_1 modulated with frequencies ν_a, ν_b and ν_c (curve with early maximum and without data points in Figure 4c,d). The residue is a doubly exponential function (time constants τ_1, τ_2) with a simple modulation (ν_d) (crosses and the unmodulated curves with late maxima in Figure 4c,d; shown also in a linear scale in Figure 4e,f), which describes filling up a location L_2 from L_1 (with time constant τ_1), an oscillation in this region and the depletion of L_2 (lifetime τ_2). Figure 4c,d shows how these two contributions (from L_1 and L_2) add up to the total signal (from which the Rydberg contribution has been subtracted). Figure 4e,f displays the L_2 contribution once more (crosses), the result of dividing it by the doubly exponential fit and, in the inset, the Fourier transform of this oscillatory part. Obviously, there is only a single oscillation frequency. As before, it was used in the time-dependent fit functions to simulate the periodic parts and the partial and total signals, as shown in Figure 4.

The $C_2H_3^+$ ($C_2D_3^+$) fragment signal looks similar in this time range as the $C_2H_2^+$ ($C_2D_2^+$) signal (which has a better signal-to-noise ratio) and does not contain additional information. This short-time part is therefore not shown.

At longer times, in the picosecond range, the two fragments reveal very weak tails, nonmodulated exponential decays with

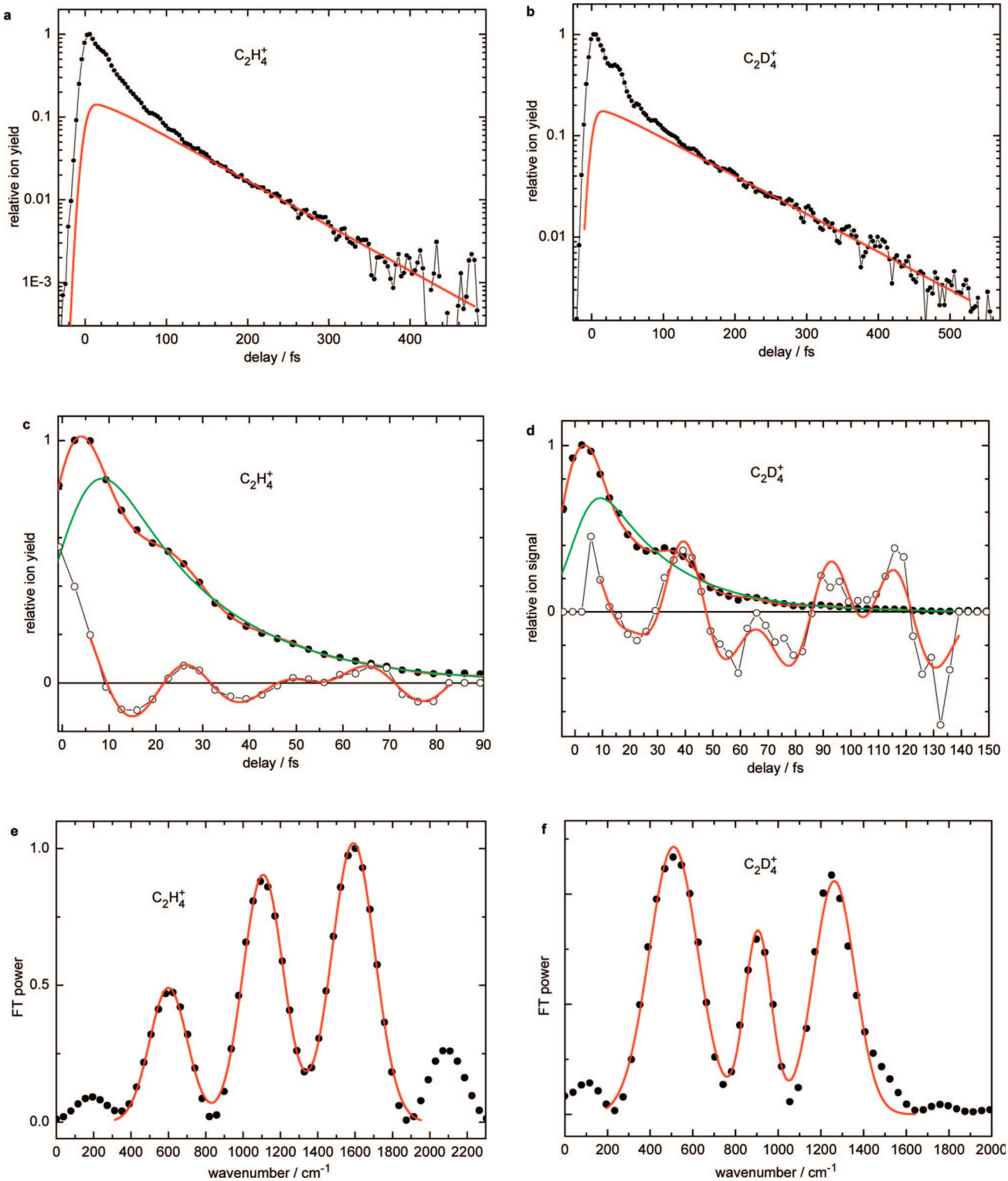

Figure 3. Parent ion signals. (a, c, e) $C_2H_4^+$; (b, d, f) $C_2D_4^+$. (a, b) Full signals and a simulation of the Rydberg-path contribution (fit to the slower decay, time constant τ_R, supplemented by an exponential, rising with τ_1; with convolution). (c, d) Signal (full symbols and signal simulation by the full-fit curve) after subtraction of the Rydberg-path contribution and a singly exponential fit (with convolution; lifetime τ_1); dividing these data by the fit curve and subtracting 1 results in the open symbols, which is fitted by a product of oscillatory function of type (1) (oscillation frequencies ν_a, ν_b, ν_c). (e, f) Fourier transforms (dots) of the oscillatory functions in (c) and (d), fitted with the sum of three Gaussians.

time constants τ_3 and τ_4. To detect them, we raised the probe intensity by a factor of 3 (to $\approx 10^{14}$ W cm^{-2}) and the pressure up to $\approx 10^{-4}$ mbar (from the normally used 10^{-7} to 10^{-6} mbar) and did more averaging. They are shown in Figure 5. Whereas the $C_2H_3^+$ signal shows both τ_3 and τ_4 (the latter more clearly, Figure 5a,b), the fragment $C_2H_2^+$ only contains τ_3 (Figure 5c.d) The effect of the probe intensity is demonstrated with $C_2D_3^+$ as an example in Figure 5b, where the small symbols show data recorded with standard probe intensity ($\approx 3 \times 10^{13}$ W cm^{-2}). Evidently, reducing the intensity by a factor of 3 lowers the ion yields to levels, where τ_3 can barely be recognized and the τ_4 window (L_4) is below the detection limit.

The parent-ion signal decays to 0. That is, the ion yields at negative and long positive delay times coincide. The former is

TABLE 1: Lifetimes τ_i of Population in the Locations L_i, Ionization Cross-Sections ${}^m\sigma_i$ To Produce an Ion of Mass m (m in Parentheses in Column 1) from L_i and the Oscillation Frequencies from L_i[a]

L_i (C_2H_4): τ_i:	L_R 80 fs	L_1 21.4 fs	L_2 16.5 fs	L_3 0.60 ps	L_4 5.0 ps
$C_2H_4^+$ (28 u)	0.1	1	0	0	0
	0.07	*1*	*0*	*0*	*0*
$C_2H_3^+$ (27 u)	0.08	1	0.3	0.004	0.003
	0.2	*1*	*2.3*	*0.018*	*0.008*
$C_2H_2^+$ (26 u)	0.07	1	0.7	0.001	0
	0.08	*1*	*1.6*	*0.002*	*0*
ν/cm^{-1}		631, 1113, 1572 (ν_a, ν_b, ν_c)	1263 (ν_d)		
L_i (C_2D_4): τ_i:	L_R 115 fs	L_1 24.2 fs	L_2 21 fs	L_3 1.6 ps	L_4 11 ps
$C_2D_4^+$ (32 u)	0.1	1	0	0	0
$C_2D_3^+$ (30 u)	0.2	1	4.2	0.01	5×10^{-5}
	0.1	*1*	*1.2*	*0.026*	*0.006*
$C_2D_2^+$ (28 u)	0.1	1	2.7	0.002	0
	0.1	*1*	*2.5*	*0.007*	*0*
ν/cm^{-1}		512, 891, 1263 (ν_a, ν_b, ν_c)	1190 (ν_d)		

[a] Estimated error limits for the time constants and frequencies are ±5%. The ${}^m\sigma_i$ values printed in italic are for a probe intensity of $\approx 10^{14}$ W cm^{-2}, the others for $\approx 3 \times 10^{13}$ W cm^{-2}. The picosecond time constants τ_3 and τ_4 were determined with the higher intensity, which raises the corresponding signals (Figure 5b).

obviously due to multiphoton ionization by the probe; it was subtracted from the measured data. For the fragment ions the long-time signals are slightly higher (about 10^{-4} of the maximum) than those at negative time. Because this "pedestal" depended nonlinearly on the UV intensity (varied by a factor of 2, by changing the pressure in the Ar cell), it cannot be due to one-photon excited molecules; therefore we subtracted the pedestal from the fragment signals. All the rest, i.e., the signals from all L_i, are linear in the *pump* intensity and the ratios of signals stay perfectly constant. The absence of a long-time signal means that no end product was detected.

The *probe* energy was also varied (by a factor of 3, Table 1). An example is also shown in Figure 5b. The corresponding variation of the signal intensity (more precisely: the ionization probability) could inform on the order of ionization of the different L_i and hence on their relative energies. For this purpose, one should add up the parent and fragment signals; unfortunately, each signal was separately measured and normalized. We instead compare the dominant signals: the parent from L_1 and L_R, and $C_2H_2^+$ from L_2 and L_3. The former pair was found to have the same order of ionization (the signal ratios do not change with the probe energy, Table 1), so that the two locations have roughly the same energy. As to L_3 and L_4, the probe-intensity dependence is less conclusive, probably because the fragmentation pattern also changes with the intensity. Nevertheless it can be recognized from Table 1 that L_3 and L_4 are below L_2, because the signals from the former are by more than 2 orders of magnitude weaker than those from L_2. Also the fragment intensity from L_1 relative to that from L_2 should not be used for conclusions, because fragmentation in the former is very minor and certainly intensity dependent, whereas from L_2 the fragments dominate. In section 4.2 we conclude from the drastic increase of fragmentation that L_2 is much below L_1.

One could expect that the ${}^m\sigma_i$ from corresponding locations L_i coincide for the two isotopomers. This is the case within a factor of 2 for the higher probe intensity (Table 1). For the fragments at lower intensity there are more deviations, perhaps due to their strong sensitivity to the intensity. (The intensity might have been slightly different from day to day.)

In the context of the isotope shifts, the error limits of the time constants and frequencies would be interesting. In previous experiments we used for this purpose the standard deviation found, when each of ≥10 scans was evaluated and the results averaged. In the present case this is difficult, however, due to the multistep evaluation procedure (subtraction of the L_R contribution, for L_2 also subtraction of the L_1 contribution, division by the exponential parts, etc.); as a consequence not only is the analysis of each scan tedious, but the errors of the different quantities will also be interdependent. Nevertheless, to get an estimate at least for the more important numbers (τ_1, τ_2 and the vibrational wavenumbers), we instead averaged the measured *data* of 8 scans each and then evaluated them. Then the same was done with another such set (for C_2H_4 it was measured at the higher probe intensity, for C_2D_4 on another day) and the results compared. The (±) deviation from the average was

−for C_2H_4: 3% for τ_1 and τ_2; 5%, 0.5%, 1% and 3% for ν_a−ν_d

−for C_2D_4: 4% for τ_1; 0.6% and 3% for ν_a and ν_b

In view of the small deviations it is probably safe to estimate an error limit of ≤5%, also for the time constants and wavenumbers, for which the fluctuation was not investigated.

4. Discussion

4.1. Generation of the Short 162 nm Pulses. It was previously considered difficult to produce short pulses in the deep UV or even vacuum UV. In this region the refractive-index dispersion of windows, nonlinear crystals and even of gases is larger than at longer wavelengths; it gives rise to chirping and pulse lengthening. Compression methods for chirped pulses in the UV are not yet satisfactory (see, e.g., the limited success with a prism compressor in ref 66) and would first require some development (such as that using flexible mirrors[70]). Our method generating the third[66] or fifth harmonic[65] in a short gas cell, which introduces only little dispersion, leaves the duration of the pulses unaffected, or even shortens them a little due to the nonlinearity of the process. (It was shown in ref 66 that even tunable radiation can be generated in a variant of such a setup.) Starting with pulses of 700 μJ and 12 fs at 810 nm, we obtained 11−12 fs pulses at 162 nm with an estimated energy of 4 nJ, with still some room for optimization.[65] It was enough to pump ethylene. Its absorption cross-section in this region ($\sigma \approx 3 \times 10^{-17}$ cm^2, Figure 1) implies a saturation energy density of $h\nu/\sigma = 40$ mJ cm^{-2}; 0.3% of it (section 2) will excite 0.3% of the molecules. This requires only mild focusing (to 3×10^{-3} mm^2, which is the focus cross section estimated in section 2). This energy and the percentage of excited molecules was even sufficient to detect very weak signals such as those originating from molecules after their return to the ground state (section 4.2.3); for ionization from there, five more probe photons are required than from the Franck−Condon region. Previous experiments[59−62] did not detect such signals.

Short time constants can in principle also be extracted by deconvolution from measurements with longer pulses, and this has been done in the previous experiments on the dynamics of ethylene;[59−62] if several linearly independent (ion) signals are available, more than one such constant can be deduced.[63,69] The potential and limitations of this method are discussed in ref 69. But high-frequency periodic oscillations cannot be extracted by

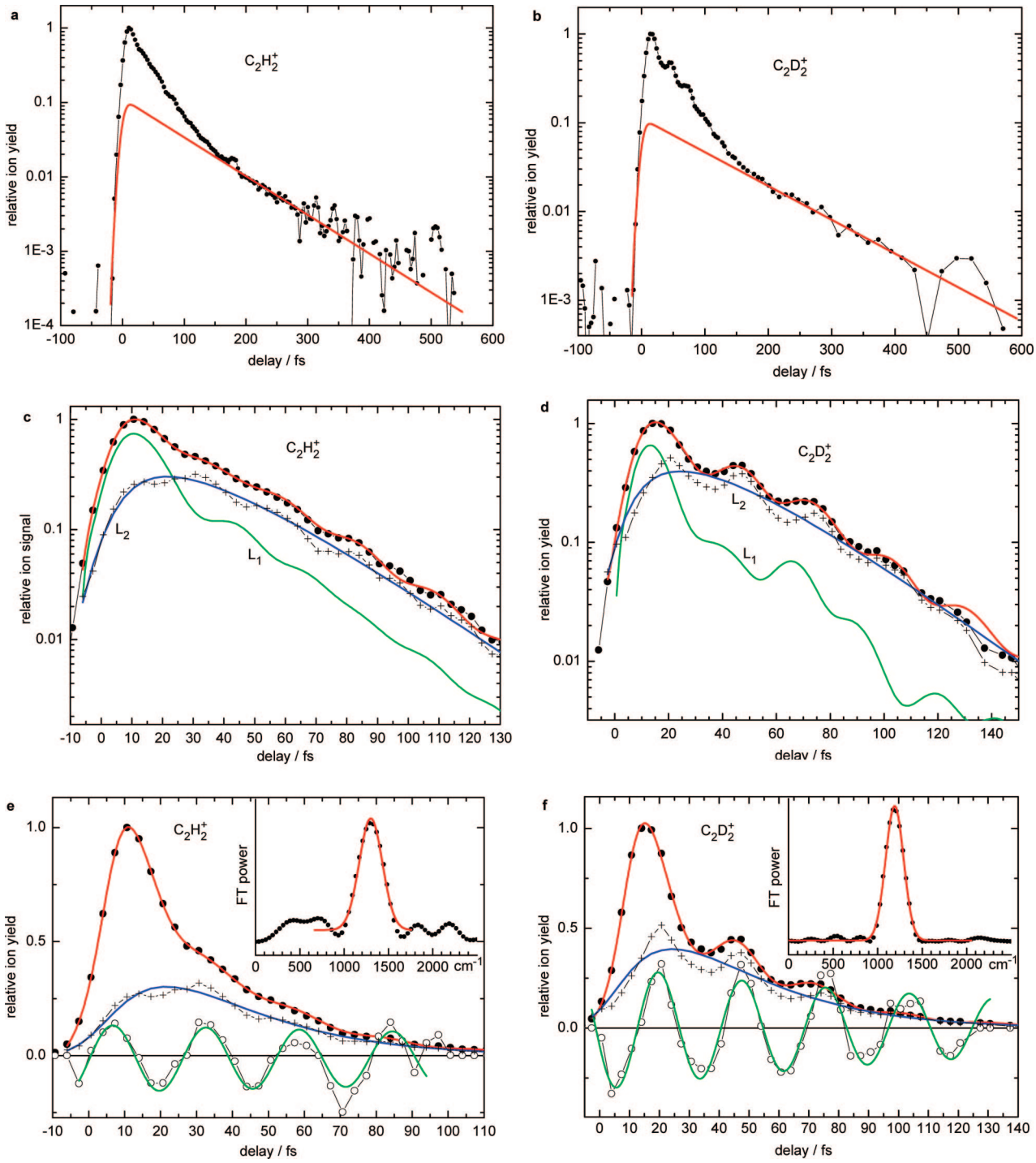

Figure 4. Fragment ion signals. (a, c, e) $C_2H_2^+$; (b, d, f) $C_2D_2^+$. (a, b) full signals and a fit curve to the slower decay (time constant τ_R, with convolution). (c, d) Signal (full circles) after subtraction of the slower decay, simulated by the full-fit curve; subtraction of the L_1 contribution (curve with early maximum) yields the L_2 contribution (crosses), which is fitted by exponentials (time constants τ_1, τ_2, with convolution). (e, f) The data after subtraction of the Rydberg contribution (full circles) and after subtraction of the L_1 contribution (crosses) and their exponential simulation are again shown; dividing the L_2 data by the fit curve (minus 1) results in the oscillatory part (open circles), whose Fourier transform is plotted in the inset; their simulation by a function of type (1) is also shown.

deconvolution. To detect them, short pulses are needed. It is shown also in this work how much information is obtained from such oscillations.

4.2. Assignment of Time Constants and Oscillation Frequencies. The observation windows L_i are locations (regions) on the potential surfaces, which are to be identified by the assignment. The evaluation in section 3 has delivered population lifetimes τ_i for them and for some L_i also oscillation frequencies. The L_i are also associated with different mass spectra (fragmentation patterns), ionization probabilities and orders of ionization, and these properties help to assign the L_i to different locations or regions on the potential surfaces: Electronic relaxation lowers the electronic energy and therefore reduces the ionization probability (*signal intensity*) and raises the *order of ionization*; the latter is determined from observing the signal on variation of the probe intensity. Because the total energy is conserved during relaxation, vibrational excess energy is released, and ionization of such a hot molecule gives rise to a

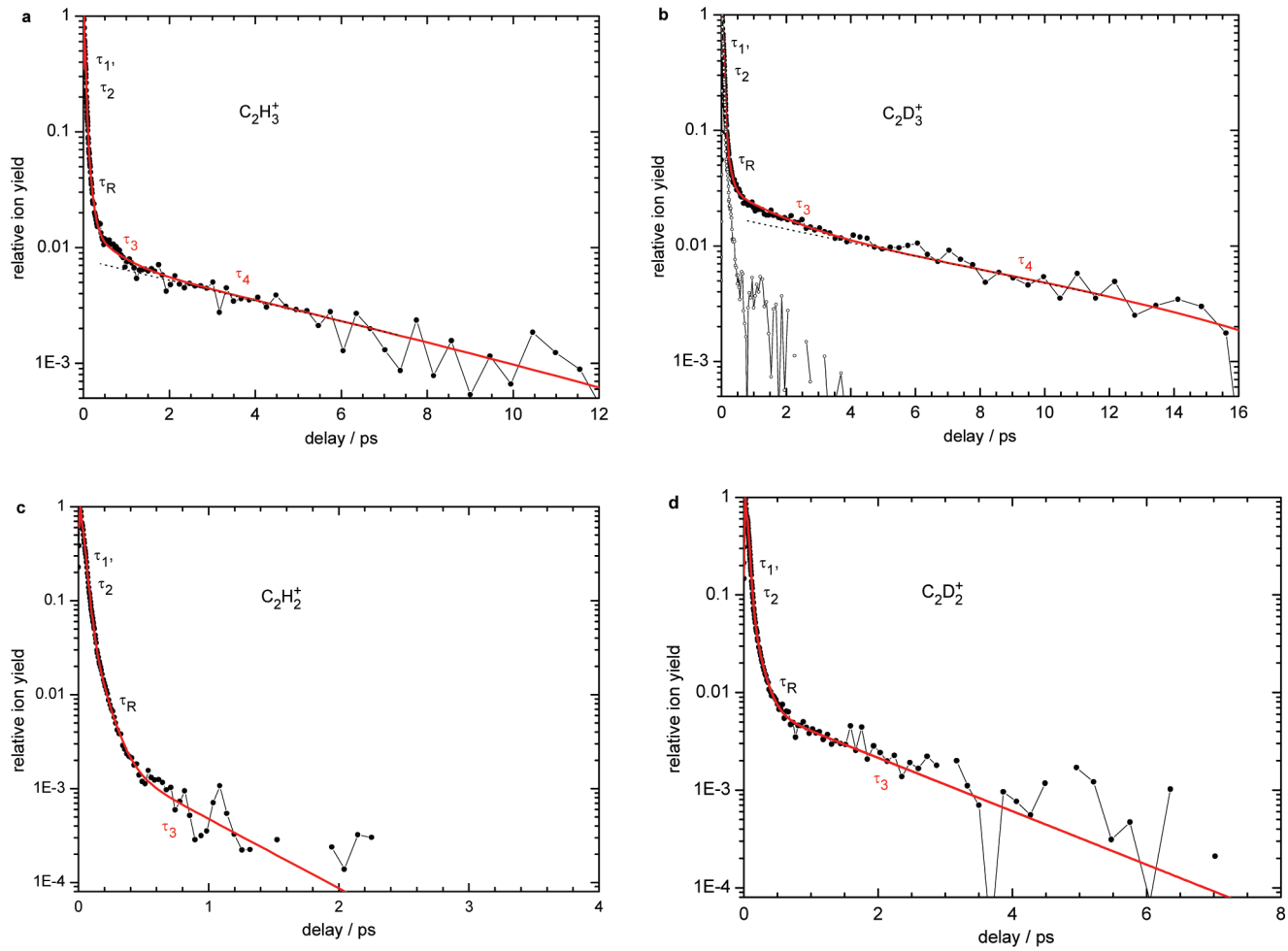

Figure 5. Signals of fragment ion signals (as indicated) at longer times, showing the time constants τ_3 and τ_4. The shorter time constants τ_1, τ_2 and τ_R are derived from the signal parts in Figures 3 and 4. Note that the time scales are different. τ_4 shows up only in the $C_2H_3^+$ ($C_2D_3^+$) signal. The data were recorded with ≈3 times higher probe intensity (≈10^{14} W cm^{-2}) than usual, which improves the signal-to-noise ratio significantly; as an example, data for standard probe intensity are also shown for $C_2D_3^+$ (small open circles).

hot ion that fragments before detection; the *degree of fragmentation* is thus also a measure of the electronic (or vibrational excess) energy of an individual L_i. The fit parameters ${}^m\sigma_i$ reflect both the ionization probability and the fragmentation pattern (for details see ref 63).

Coherent oscillations can also help to identify the L_i, if independent spectroscopic information is available. They result from superposition of stationary vibrational states of the molecule in the location L_i. However, there is a chance to observe an oscillation only, if the vibration modulates the ionization or fragmentation probability. This is not expected, for example, if in the probe transition the lower and upper potentials are parallel, as is the case on ionization from a Rydberg state. There are also a number of other reasons why some oscillations may remain unobservable.[68]

For the assignment we start with knowledge of the potentials from spectroscopy and quantum chemistry (Figure 6). Initial excitation at 162 nm mainly populates the one-electron excited $\pi\pi^*$ (V) state (symmetry B_{1u} in D_{2h} if the z axis is chosen[2] to coincide with the CC bond and the x axis perpendicular to the molecular plane). According to Figure 1, the lowest Rydberg state (π3s or R3s, B_{3u}) state is excited in parallel with about 5−10 times less probability. The π3s state is slightly lowered on CC twisting, reaching a minimum near 25−30° [71] and rising again beyond. On the other hand, the $\pi\pi^*$ potential is lowered by about 2 eV[8] from the Franck−Condon region (7.7 eV) by

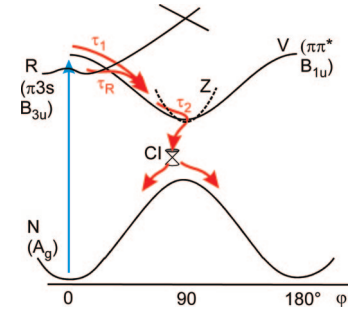

Figure 6. Initial dynamics and potentials including the Rydberg π3s state and the zwitterionic (Z, π^{*2}, totally symmetric) state. φ is the C═C torsion angle. The conical intersection (CI) is out of the drawing plane.

twisting by 90°. The two potentials intersect each other at a torsional angle of ≈35°.[20] Therefore population can flow easily (i.e., with only very minor activation energy) from the Rydberg π3s state to the $\pi\pi^*$ surface and from there further down (Figure 6).

According to the present understanding,[17] the way down from the Franck−Condon region of the $\pi\pi^*$ state involves not only CC torsion φ (which gives rise to a horizontal tangent at φ = 0 and hence to only slow initial acceleration) but also CC stretching. The latter is not indicated in Figure 6. Near φ = 90°, the V and Z states become nearly degenerate and easily

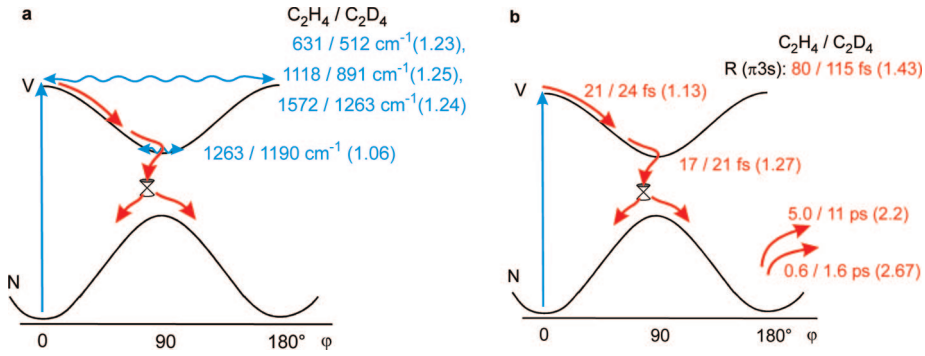

Figure 7. Isotope effect (ratios in parentheses) on the vibrational wavenumbers (a) and the time constants (b). The lifetimes for the Rydberg state (τ_R) are only listed (illustrated in Figure 6). The path for the ground-state processes is assigned in section 4.2.3.

exchange population. After reaching $\varphi = 90°$, the molecule takes a new relaxation direction to reach a conical intersection (CI) with the ground-state (S_0) surface. The new direction involves pyramidalization of one CH_2 group and/or partial migration of an H atom from one C to the other (see Introduction). After passing through the CI, the molecule can either directly reach the S_0 minimum of C_2H_4 or, if H migration is involved, temporarily arrive at a structure corresponding to the carbene CH_3CH (ethylidene, not indicated in Figure 6). Ethylidene very rapidly rearranges on a barrierless path in the ground state back to ethylene (section 4.2.3). In the hot S_0, H and H_2 eliminations can take place (section 4.2.3).

4.2.1. Franck−Condon Region. The parent-ion signal contains strong contributions from observation windows (L_R and L_1) with time constants τ_R and τ_1, whereas it does not show the time constants $\tau_2-\tau_4$. That is, from these locations L_R and L_1 the ionization probability is highest, and fragmentation probability is lowest. Obviously they represent the Franck−Condon region. The signal contribution from L_R is about 10 times smaller than that from L_1. This is practically the same as the estimated ratio (5−10) of excitation probabilities of the $\pi\pi^*$ and π3s states (see above and Figure 1). Therefore we assign L_R to the Rydberg π3s state (lifetimes τ_R = 80 and 115 fs for C_2H_4 and C_2D_4, respectively) and L_1 to the $\pi\pi^*$ state (lifetimes τ_1 = 21 and 24 fs, respectively) (Figure 6). This assignment is supported by the oscillations, which are observed in the τ_1 window but not in L_R: Although vibrational coherence is certainly also generated on exciting the Rydberg state, it should not be observed on probing by ionization, because of the parallel potentials, as explained above.

On excitation of the $\pi\pi^*$ state, a coherent superposition can be expected for Franck−Condon active vibrations. This will be mainly the torsion (twist, ν_4) and probably also the CC stretch (ν_2); the resonance-Raman spectrum also suggests some activity of the symmetric scissors vibration (ν_3) and its antisymmetric counterpart (ν_{12}) and out-of-plane wagging (ν_7).[9,10] In S_0, full deuterium substitution reduces all these frequencies by a factor of 1.41−1.33 except the CC stretch vibration (ν_2), which is reduced by a factor of 1.07,[72] as the inverse ratio of the square root of the moving masses. For the coherent oscillations ν_a, ν_b and ν_c observed in the $\pi\pi^*$ state (L_1) the corresponding factors are 1.23, 1.25 and 1.24, respectively (Table 1, Figure 7a). Hence not one of them involves a pure hydrogen vibration; all must be mixed and contain some CC stretch. From the wavenumbers one may suppose that the CC stretch dominates in ν_b (1110 cm^{-1} in C_2H_4); then the torsion will dominate in ν_a (630 cm^{-1} in C_2H_4), and ν_c (1570 cm^{-1} in C_2H_4) will be the combination vibration of the two. The latter wavenumber would be too high to assign it to a CC stretch (ground-state value 1623 cm^{-1},[72] which should be drastically reduced in a π-antibonding state). The wavenumber of ν_c is by 9% smaller than the sum $\nu_a + \nu_b$, which is in the range of common anharmonic shifts.

This assignment is also supported by the recurrence times of the wave packets calculated after excitation to this energy region by Viel et al. and Brill et al.:[12,34] The CC distance oscillates with a period of 25−30 fs, corresponding to a wavenumber of 1330−1110 cm^{-1}; the torsion has a recurrence time near 45 fs (740 cm^{-1}). The calculation also predicts a small amplitude for the scissors vibrations (similar frequency as CC stretch; but note that we need a strong participation of the CC stretch vibration to explain the small isotope shift that we observed) and a practically negligible amplitude for wagging. The calculation further points out that the CC distance shortens on twisting (after lengthening at the initial zero twist), so that the two motions are not separable. This can explain the mixed character of the vibrations, concluded above from the small isotope shift, and also the observation of a combination vibration. Interestingly, Barbatti et al. find in their surface-hopping study a periodicity of ≈20 fs (1660 cm^{-1}, well consistent with our combination vibration of 1570 cm^{-1}) in the S_1 population, if excited at 160 nm (Figure 4 in ref 35); because V ↔ Z relaxation only takes place at a certain geometry (near $\varphi = 90°$), this periodicity must reflect a vibration, which contains the torsion. Our findings thus also confirm the quantum chemical calculations of.[12,34,35]

In the spectra (Fourier transforms, Figure 3e,f) of the oscillations in the Franck−Condon regions the relative intensity of the combination frequency over that of the fundamentals is not the same for C_2D_4 and C_2H_4. This is not unexpected, if the anharmonic interaction between CC stretch and torsion differs for the two isotopomers. Such interactions usually depend on frequency differences and hence on isotopic substitution. Probably one can interpret in the same way the different intensity ratios of CC stretch (which is weak in C_2D_4) over that of CC torsion (which is weak in C_2H_4). The narrow width of the CC stretch of C_2D_4 (Figure 3f) is probably an artifact of the Fourier transform, because it is not reflected in the dephasing time in the simulation of the time-dependent data. Also the peak near 2100 cm^{-1} for C_2H_4 may be spurious, although it would fit to the next member ($v_4 = 2$) in the sequence $\nu_2 + v_4\nu_4$.

The isotope effect on the time constants (Figure 7b) will be discussed in section 4.2.5.

4.2.2. Departure from S_1. The time constant τ_2 is not contained in the parent-ion signal but only in the two fragments. This means that from L_2 ionic fragmentation is complete (in contrast to L_1 and L_R, from which the parent ion dominates, Table 1), indicating that L_2 is much lower in energy than the Franck−Condon region. Because the next two windows (L_3 and L_4) are already on the S_0 surface (section 4.2.3), τ_2 must be the

time for leaving S_1. The oscillation observed in L_2 ($\nu_d = 1260$ and 1190 cm^{-1} for C_2H_4 and C_2D_4, respectively) must then be a vibration in the lower part of the S_1 surface. The isotope shift (6%) indicates that it is a pure CC stretch vibration. Interestingly, Foo and Innes found in the long-wavelength part of the UV spectrum of C_2D_4 a progression displaced by 1250 cm^{-1} from the main (ν_4) progression.[8] They assign this shift to a ν_2 quantum, i.e., to a CC stretch vibration in the lower part of S_1. The agreement with our 1190 cm^{-1} seems to us good enough (see end of section 3 for the estimated accuracy) to support our identification of ν_d and location L_2 (see next paragraph, however). Furthermore the increase of the CC stretch wavenumber from L_1 to L_2 (ν_b compared to ν_d) by 15−30% is fully consistent with the theoretical prediction[12,19−21] that the CC bond is shorter at $\varphi = 90°$ than at 0°, implying a stronger bond in the twisted structure. It is even more strengthened and shortened, when an H bridge forms on the way to H migration.[20]

The agreement of our CC stretch frequency with the spectroscopic value for the region near the perpendicular S_1 "minimum" (C_2H_4 with D_{2d} symmetry) does not necessarily mean that our L_2 is exactly there. If τ_2 is the time for leaving S_1, L_2 should extend to the S_1/S_0 CI; a change of ionization probability (hence a termination of the observation window L_2) will take place especially there, where the electronic energy quickly drops and the electronic state is changed. Hence in L_2 there will also be some pyramidalization and/or H migration in addition to the 90° torsion. In fact, quantum chemistry predicts that the D_{2d} structure is not a minimum (which would imply some residence time) but a saddle point.[19,21,26,27]

During a drastic geometrical change such as pyramidalization and/or H migration any initial twist vibration will strongly change its character and wavenumber (from an initial value near 800 cm^{-1} in the D_{2d} geometry[7,8]). Furthermore, near this structure the zwitterionic state begins to be populated, in which the twist vibration has a much higher frequency (note the strong curvature of the Z potential in Figure 6). Any initial coherence would be rapidly lost by such frequency variations. It is therefore not surprising that a coherent twist oscillation (ν_4) and its combination with CC stretching (ν_2) is not observed from L_2. (In fact, a ν_4 oscillation has been observed in S_1 of C_2F_4, where the zwitterionic state seems to be higher in energy and not involved in the relaxation process.[73]) It is also not surprising that any ν_2/ν_4 mixing is completely different between the two windows L_1 and L_2, as indicated by the different isotope effect. In L_1 the twist is a hindered free rotation; along the large angular excursion the CC distance changes (see above) so that the two motions couple. In L_2 the twist amplitude is much smaller (Figures 6 and 7a), so that the CC distance remains constant and the two motions are decoupled.

In a previous investigation of the ultrafast dynamics of ethylene (pumping by 130 fs pulses at 198 nm), Stert et al.[62] also found a second time constant with values ($\tau_2 \approx 15$ and 25 fs for C_2H_4 and C_2D_4, respectively) very similar to ours. The cutoff in the photoelectron spectrum, measured by a coincidence technique from this window, indicates that the probe laser (792 nm, 1.56 eV) does not reach the energy minimum of the parent ion but a higher state. Indeed, the electronic ground state of the ion is raised by geometric distortion. In Figure 8a, we adopt the calculated ion energies of 1.3 eV (above the ion ground state) for D_{2d} (perpendicularly twisted) geometry[74] and the value 1.2−1.4 eV calculated for CH_3CH^+ or a bridged variant of it;[75] these energies are 11.8 eV above neutral C_2H_4. Using the 0.85 eV cutoff energy of the photoelectrons in five-photon ionization,[62] we obtain an electronic energy of L_2 of 4.8 eV (Figure 8b). (We tacitly assume ionization with $\Delta v = 0$, i.e., parallel potentials for the neutral molecule and ion in this region. This assumption seems necessary to explain the sharp cutoff observed.) This value is entirely conceivable for the region between the perpendicular D_{2d} minimum (5.5 eV[8]) and the S_1/S_0 CI; furthermore, it is fully consistent with the twisted-pyramidalized CI of 4.5 eV of the recent high-level calculations[20] (see also Figures 5 and 6 there[20]). This experimental evidence hence also supports the assignment of L_2 to a region extending to the last CI from around the D_{2d} minimum. Furthermore, we can conclude on the molecular structure in L_2 before reaching the CI: Because the photoelectrons were measured in coincidence with the $C_2H_2^+$ signal and because H_2 elimination from the $C_2H_4^+$ *ion* takes place only after partial or complete H migration,[74,76] such a rearrangement must have happened in the neutral molecule, too, before vertical ionization. A similar conclusion on the structure *after* passing the CI is drawn in the next section.

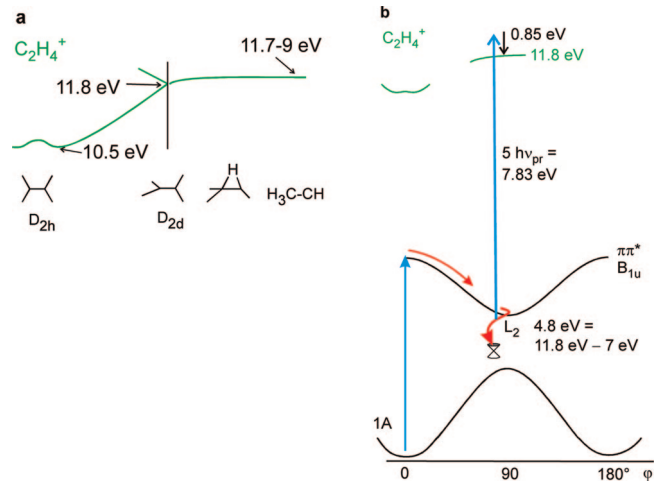

Figure 8. (a) Ion energies relative to the neutral ground state. In D_{2d} geometry (calculation by Sannen et al. [74]), the electronic state is degenerate. From there, H migration does not much affect the energy according to the calculation of Oblinger et al.[75] (b) Taking the ion energy (11.8 eV) from (a) and the photoelectron cutoff energy of 0.85 eV, one calculates the L_2 energy to 4.8 eV.

4.2.3. Ground-State Processes. The signal parts with long time constants τ_3 and τ_4 (reflected in the tails of the two fragment ion signals, Figure 5) are already very weak, for both fragments by 2−3 orders of magnitude weaker than from L_2 (Table 1, Figure 5). This indicates that ionization from L_3 and L_4 requires 1−2 more photons for ionization than from L_2. (This conclusion is supported by the probe-intensity dependence of the $C_2D_2^+$ and $C_2D_3^+$ signals; the latter is illustrated in Figure 5b. The evidence from the nondeuterated signals is not so clear-cut however.) So, τ_3 and τ_4 are most probably time constants of reactions in the hot ground state. (See the end of this section for an interpretation, why both signals decay to 0.) Several reactions are known from hot C_2H_4 resulting after internal conversion:[40,41]

The branched first step in this scheme can give rise only to one observable time constant (inverse of the sum of the three rate constants), which would be the lifetime of the hot ethylene. The subsequent (exothermic) step in (2a) would be too fast to be observed after the slow (strongly endothermic) first step. Although the second step in (2b) (less endothermic than the first) is energetically not accessible at 193 nm, RRKM calculations predict that it is 8−12 times faster than the first with the excess energy available with 157 nm (7.9 eV) excitation.[52] This

SCHEME 1: Ground-State Reactions of Hot Ethylene

H_2CCH_2 → $H_2CC + H_2 \rightarrow HCCH + H_2$ (2a)
$H_2CCH + H \rightarrow HCCH + 2H$ (2b)
$H_3CCH \rightarrow$ ..... (2c)

SCHEME 2: Ground-State Reactions of Hot Ethylidene

H_3CCH → $H_2CCH_2 \rightarrow$ ..... (3a)
$HCCH + H_2$ (3b)
$H_2CCH + H \rightarrow$ ..... (3c)

is probably similar to our 162 nm (7.65 eV), so that also this step will not be observed. Similar considerations apply to the third line, because CH_3CH decays primarily back to ethylene (see below), faster than it is formed. So only one of the two time constants τ_3 and τ_4 can be explained by Scheme 1.

Here one should recall the possibility that CH_3CH forms not only from ethylene (reaction 2c) but also directly from the S_1/S_0 CI. If this is the case, this path is much faster (17 fs) and kinetically independent from reaction 2c. Ethylidene rearranges rapidly to ethylene[77] in a nearly barrierless[78,79] process; but H_2 and probably H elimination from it is also observed (Scheme 2).[78] This means that dissociation is competitive with rearrangement.

The three reactions will again give rise to only one observable time constant. It is independent of that characterizing reactions 2. We conclude that already the fact that two ground-state time constants (τ_3 and τ_4) are observed points to formation of ethylidene directly from the CI, independently of the path (2c).

Reaction 3a is strongly exothermic (by ≈3 eV[80]) and barrierless or nearly so.[78] We can expect that it is faster than the endothermic reactions (2). This is confirmed by RRKM calculations, which predict rates of $(6-8.5) \times 10^{12}$ s^{-1} for it.[52] Therefore we assign our τ_3 to the lifetime of hot CH_3CH (caused by the set of reactions (3)) and our τ_4 to the lifetime of hot C_2H_4 (set of reactions (2)).

This assignment is also supported by the fact that the longer time constant (τ_4) is only contained in the $C_2H_3^+$ signal but not in the $C_2H_2^+$ signal (Figure 5). This point shall be explained by Figure 9: It is generally accepted that H_2 elimination from the $C_2H_4^+$ ion takes place only after hydrogen migration, i.e., from the ethylidene ion (left-hand side in Figure 9).[74,76] Hence vertical ionization of hot CH_3CH will reveal its short lifetime (τ_3) in the $C_2H_2^+$ ion (also in the $C_2H_3^+$ ion, see Figure 9), whereas from ethylene in its hot ground-state (lifetime τ_4) vertical ionization and subsequent fragmentation will primarily lead to $C_2H_3^+$, so that τ_4 will be detected only in this signal, as is indeed the case (Figure 5). (Such a preferential elimination of H over that of H_2 was also found, when $C_2H_4^+$ was generated as $H_2CCH_2^+$ with D_{2h} structure by multiphoton ionization that was two-photon resonant with Rydberg states.[81]) This also means that the ionic dissociation is kinetically controlled; if it were thermodynamically controlled—i.e., only by the excess energy, independent from which location on the potential it starts—both channels would be equally probable, because the appearance potentials of the ions $C_2H_3^+$ (13.22 eV) and $C_2H_2^+$ (13.14 eV) are practically identical.[82] Also our observation of different kinetics of the $C_2H_2^+$ and $C_2H_3^+$ signals points to kinetic control of $C_2H_4^+$ dissociation.

The D isotope effect on τ_4 is larger (2.2, Figure 7b) than for a barrierless hydrogen motion (1.41) but probably consistent with the assignment to the endothermic H elimination. Also the D effect on τ_3 (2.67) indicates an activated process. Perhaps

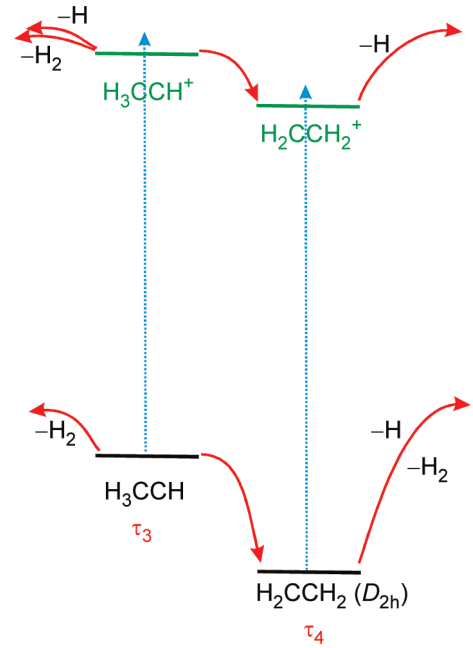

Figure 9. Fragmentation in the ion is slightly different from that in the neutral molecule: H_2 elimination takes place only from H_3CCH^+. The lifetime (τ_4) of hot ethylene will therefore not appear in the $C_2H_2^+$ signal.

this is because the (endothermic) H_2 elimination contributes to τ_3. It indicates that also the ethylidene → ethylene rearrangement by H migration is not completely barrierless, although some calculations predict that.[78] A minor barrier seems to us consistent with some photochemical observations (see below). It is also suggested by a similar deuterium effect (3.2) for H migration in the homologue dimethylcarbene at room temperature in pentane.[77] In the same work[77] a lifetime of CD_3CD of 500 ps was deduced, on the basis of the assumption of a rate for the scavenging reaction; because this lifetime is by 3 orders of magnitude longer than ours, we suppose that the scavenging process in ref 77 probably took a different path.

With the given interpretation, all the hot ground-state products (ethylene and ethylidene) will eventually end in acetylene (reactions 2 and 3). It will certainly still have some excess energy. It is well conceivable that this end product was not detectable, because (1) it has an even higher ionization energy (11.4 eV) than ethylene (10.5 eV),[83] so that one more photon (altogether 8) would be needed for ionization, and (2) with the available excess energy it would fragment after ionization, so that its signature would only appear in lower-mass fragment ions that were not investigated. It is therefore not surprising why the $C_2H_3^+$ and $C_2H_2^+$ signals both decay to 0.

We can now summarize the main basis of the assignment of the L_i: L_1 and L_R are the two states ($\pi\pi^*$ and Rydberg π3s) directly populated by the primary excitation, as known from spectroscopy. L_2 is a state much lower in energy, as indicated by the drastic change of the fragmentation pattern (no parent ion from L_2); this location probably extends from the V−Z intersection to the last CI. Vibrational frequencies (from coherent oscillations), the time-resolved photoelectron spectra from literature and the quantum-chemical calculations are consistent with this assignment. L_3 and L_4 are locations on the S_0 surface (with CH_3CH and H_2CCH_2 structure, respectively); the main evidence is the ionization probability, which is by 2−3 orders of magnitude smaller than from L_2. The lifetimes are also in the predicted range for isomerization (CH_3CH) and dissociation

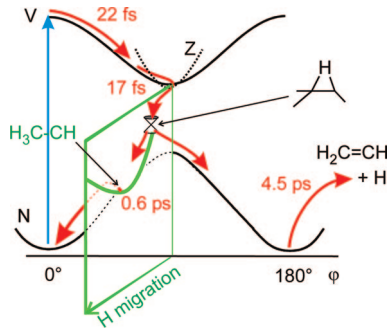

Figure 10. Potentials and dynamics of C_2H_4 (for the time constants of C_2D_4, see Figure 7b), indicating also hydrogen migration (perpendicular to the drawing plane) and the displacement of the CI into this direction. The path starting in the Rydberg state (Figure 6) is omitted. The two ground-state reactions, which were not yet assigned in Figure 7b, are now also identified. The pyramidalization of one CH_2 group, predicted theoretically,[20,21,26,27,31,32,35,37−39] is not indicated. As argued in section 4.2.5, the turn to a new direction (to H migration and pyramidalization) does not occur so sharply (as indicated) in the perpendicular minimum but begins earlier and more smoothly.

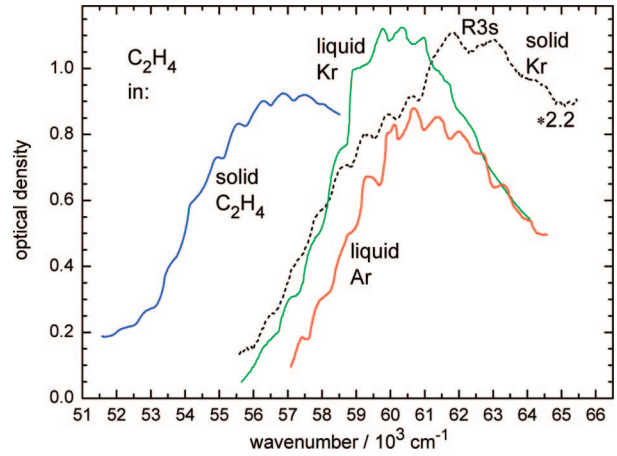

Figure 11. Ethylene UV spectra in cryogenic liquid or solid phase, as adapted from ref 85 (solid ethylene), ref 84 (liquid Ar and Kr) and ref 3 (solid Kr). Only in solid Kr can the Rydberg transition still be seen, whereas in the other spectra it is displaced to higher energies and broadened. The visible vibrational structure belongs to the $\pi\pi^*$ transition; unfortunately C_2D_4 does not reveal such a clear structure.[84]

(CH_3CH, H_2CCH_2). The expected end product (HCCH) was not detected.

In Figure 10, we summarize the complete path of the molecule from the Franck−Condon region down to the ground state. The Rydberg part (see Figure 6) is omitted from this figure. As already said, the L_1 window (departure from the Franck−Condon region) reaches down to perhaps not far from the V−Z intersection. In this region the L_2 window begins, reaching as far as to the S_1/S_0 CI. From the observation of reactions of ethylidene, we conclude that this CI is displaced from the perpendicular (D_{2d}) minimum in a direction involving H migration (outside the drawing plane of Figure 10). From the CI the path branches (1) to completion of this migration involving formation of CH_3CH and (2), on returning the hydrogen to the original carbon, to planar (D_{2h}) ethylene with $\varphi = 0$ or 180°.

4.2.4. Results of Spectroscopic Relevance. As explained in the Introduction, the UV spectrum of ethylene keeps being investigated. A difficulty is the diffuseness of the vibrational structure, in particular in the nondeuterated isotopomer. The broadening caused by the short lifetime (21 and 24 fs) is 230 cm^{-1} for C_2H_4 and 200 cm^{-1} for C_2D_4, which can be compared with the observed width of 400 cm^{-1} of vibrational peaks (near 180 nm, Figure 1; for the width at low temperature, see below) for the nondeuterated isotopomer. A certain spectral congestion seems to contribute to the widths. This is certainly also why the spectra of the two isotopomers only bear little similarity (Figure 1). Furthermore, the maximum of the $\pi\pi^*$ absorption is covered by the Rydberg π3s band with its pronounced structure, and the assumption is widespread that the $\pi\pi^*$ band below it is a continuum (Figure 1). This is not justified, however, as demonstrated by the spectra in condensed phase (Figure 11),[3,84,85] in which Rydberg transitions are broadened and displaced to higher energies: Also around the $\pi\pi^*$ maximum near 162 nm, these spectra show a clear vibrational progression (680 cm^{-1}). Unfortunately the corresponding spectra of C_2D_4 are structureless or nearly so.[84] In contrast, in our method we probe by ionization from the excited state, where the Franck−Condon factors are different from those of the $S_0 \rightarrow S_1$ transition. Therefore we can find some vibrations not detected in normal UV spectra, in particular also for the deuterated isotopomer.

At the long-wavelength end of the spectrum, there should be no congestion that could contribute to the broadening. In fact, the width found for a peak near 190 nm in C_2H_4 at −78° is ≈280 cm^{-1};[7] this implies a lifetime ≥18 fs of population near the perpendicular minimum. This is well consistent with our τ_2 and the τ_2 of Stert et al. [62] (which we attribute to departure from S_1), but less well consistent with the $\tau_1 \approx 10$ fs measured in ref[62] with excitation at 198 nm (to an energy of ≈0.7 eV above the perpendicular minimum).

There is agreement that the prominent progression is formed by CC twisting in a potential with minimum (in a cut in this direction) at 90° and maximum at 0°. In the long-wavelength wing the spacing (≈800 cm^{-1}) corresponds to one vibrational quantum near the minimum.[2−4] (Actually, each vibrational level there is double, with wave functions with and without node below the barrier.[86]) Near and beyond the spectral maximum, the structure corresponds to hindered free rotation, and for symmetry reasons[86] the spacing (≈680 cm^{-1} in a cryogenic matrix or liquid, Figure 11) must correspond to two quanta. We find for the latter region (our observation window L_1) 630 and 510 cm^{-1} for the two isotopomers, the former perhaps slightly less than in the matrix. Probably the matrix contributes to the hindering potential and thus raises the frequency. Recent calculations of the spectrum via the wave packet recurrence time found 680 cm^{-1}[112] or 650 cm^{-1}[134] for C_2H_4, very well consistent with our results. From the small deuterium effect (which was not possible to identify in the UV spectra and which was not yet investigated theoretically), we conclude that the twist in this region is actually mixed with the CC stretch (section 4.2.1). This is in agreement with the calculations,[12,19−21] which predict that the CC bond is longer at 0° than at 90°. The amplitude of the twist "vibration" in the Franck−Condon region comprises both angles and more. This is illustrated in Figure 7a.

The mixing of CC twist and stretch vibrations implies that in the latter the isotope effect should be larger than expected for a pure CC stretch. This is in fact observed in L_1 (Figure 7a), which is near the Franck−Condon region for 162 nm excitation. But in L_2 (the region from the perpendicular minimum to the CI) the observed vibration is a pure CC stretch, according to the small isotope effect (Figure 7a). (In the long-wavelength part of the UV spectrum, this vibration was only observed with C_2D_4.[8]) Near $\varphi = 90°$ the torsional amplitude is in fact much smaller than above the barrier (Figure 7a); on small

torsional excursion, the CC distance is not expected to vary much, so that the two vibrations will not couple.

Resonance Raman spectra suggest activity of more vibrations, including wagging (pyramidalization) and rocking (planar bend).[9,10] In fact, such activity is expected, if the perpendicular minimum is actually a saddle point (see Introduction) toward pyramidalization and H migration. Simulations of the UV spectrum can perhaps reveal them, if they use experimental numbers for the more evident vibrations. Our data might help in this respect. So far, the published simulations used widely different numbers for excited-state vibrations.[14,15,87−91]

4.2.5. Ultrafast Dynamics and Implications for the Potentials. The lifetime τ_R (80 and 115 fs for the two isotopomers) found for the Rydberg π3s state, excited at 162 nm (excess energy 4400 cm^{-1} over the origin), is consistent with $\tau_R \geq 100$ fs for C_2D_4 deduced from a line width near the origin[8] and a similar estimate in ref 71. A slight shortening at higher energy is expected, if there is a minor activation energy. In fact, the Rydberg potential has a minimum at a twist angle of $\varphi = 25-30°$ [71] and rises by about 1.3 eV at $\varphi = 90°$ (Figure 6). (This value is taken over from the potential of the ion.[74]) At $\varphi \approx 35°$ it intersects with the $\pi\pi^*$ (B_{1u}) state slightly above the π3s (B_{3u}) minimum, which can explain a minor barrier (Figure 6). Obviously the population can easily flow around the lower cone of the intersection (with a temporary distortion of $B_{3u} \times B_{1u} = b_{2\,g}$ symmetry, i.e., a CH_2 pyramidalization) to the $\pi\pi^*$ state and merge there with the population that has been excited directly to this state. This path seems to us evident, although in the spectroscopic literature (e.g., in refs 8 and 92) the leakage out from the Rydberg state was called predissociation. This view of merging populations has important implications for the photochemistry of olefins, where the π3s band often precedes the $\pi\pi^*$ band (section 4.2.6).

The previous experimental studies of the ethylene dynamics had less time resolution and extracted the time constants by deconvolution. With excitation at 155 nm[59] or near 200 nm,[60−62] they found $\tau_1 \leq 40$ fs,[59] 30 fs,[60] 20 fs[61] and 10 fs.[62] Our τ_1 (21 fs) is within the error limit of the first three experiments and slightly out of this limit for the last one.[62] According to refs 35 and 36, not much difference of lifetimes for different excitation wavelengths is expected. According to ref 69 there are sometimes artifacts during the pump−probe overlapping times, if the absorption for the pump is very weak (such as for ethylene at 198 nm, used in ref 62). But it is also conceivable that the observation windows are different on probing the different locations on the potential.

We assign (section 4.2.1, Figure 10) τ_1 as the time for leaving the Franck−Condon region of the $\pi\pi^*$ state and arriving in L_2, which is the region (with population lifetime τ_2) extending from around the perpendicular minimum to the S_1/S_0 CI. The same interpretation probably applies to the results of Stert et al.[62] (section 4.2.2). Near a twist of 90° one would expect (see Introduction and Figures 6 and 10) that also a zwitterionic state (Z or π^{*2}) is involved, reversibly taking over population from V ($\pi\pi^*$) and guiding it further toward the CI. We did not detect any $\pi\pi^* \rightarrow \pi^{*2}$ (V → Z) relaxation, probably because π and π^* orbitals become degenerate at $\varphi = 90°$, so that the ionization energies of the two states will not differ there; i.e., only the sum of the populations of the V and Z states is determined in our experiment.

For the excited-state lifetime we can take the sum $\tau_1 + \tau_2$ (39 and 46 fs for the two isotopomers), because after this time we see only ground-state signals. Such short times are only possible, if the path is continuous (involving no jump between surfaces), passing through a CI, and involves no barrier. This is demonstrated by a calculation without a CI, which predicted a $\pi\pi^*$ lifetime of ≈1 ns.[93,94] This is by orders of magnitude too long, implying that a CI is necessary for interpretation of the short times. (This was already pointed out in refs 47 and 61). In addition, we can conclude that there cannot be a barrier before the CI. High-level calculations of the potentials suggest a minor barrier,[19,20,27,38,39] although this might be the case only along the shown cuts of the surfaces. Excited-state lifetimes calculated on the basis of these surfaces[12,34−38] range from ≈100 to >250 fs (summarized in ref 36), whereas a method using semiempirical surfaces suggests 50 fs.[33] Only the latter value would be consistent with our $\tau_1 + \tau_2$. In the case of the ab initio surfaces,[12,34−38] it seems to us that the initial geometrical (from $\varphi = 0°$ to 90° and CC stretch) relaxation is fast enough and that the actual bottleneck in the calculations concerns the departure from S_1. If the latter step is too slow, it also influences the population in the Franck−Condon region due to the reversibility of the V−Z relaxation. Perhaps in many calculations some minor barrier before the S_1/S_0 CI causes the bottleneck (see later in this section). Also the following feature of the potentials may play a role:

The 17 fs for τ_2 seems to us so fast (the shortest time ever found for $S_1 \rightarrow S_0$ relaxation) that the absence of a barrier alone is not sufficient for explanation: If the wave packet arrived at the perpendicular minimum and then had to search around to find the new direction toward the CI, this would probably take some time, perhaps connected with some oscillations in the preceding directions. (Trajectory calculations might show that.) If, however, there were already an early (although minor) acceleration into the new direction, this time would be saved. In fact, the electronic V → Z relaxation around the CI between the two surfaces involves an acceleration toward an asymmetric (b_{1u}) scissors coordinate,[25,35] which can be interpreted as an incipient H migration, i.e., a component of the direction toward the last CI. Such minor features may still be difficult to find out by high-level calculations. For clarity, this early and smooth turn to a new direction in the τ_2 (17 fs) window is not indicated in Figure 10. An early acceleration toward the last CI has already been previously suggested to explain short lifetimes.[63,95,96] At the end of this section, we argue that in L_2 slopes in additional directions are also needed to explain other features of the relaxation process.

The small isotope effect (Table 1 and Figure 7b) observed (and already found in ref 62) in both τ_1 and τ_2 is remarkable. It means that during both phases not only hydrogen moves (e.g., along a twist coordinate) but also CC stretching or contraction is strongly involved. Hence the small isotope effects in the lifetimes and in the vibrations are likely to have the same origin: As already explained in the context of the vibrations (sections 4.2.1 and 4.2.4), according to the calculations[12,19−21] in the Franck−Condon region (L_1) the CC bond length initially expands and then toward $\varphi = 90°$ contracts again and does so further on the way to a H-migration CI. It would be desirable to check by calculating the dynamics also of C_2D_4 whether this feature is responsible for the small deuterium effect for lifetimes and vibrational frequencies. In the previous experiment of Stert et al. (which had less time resolution), the deuterium effect on τ_1 and τ_2 was also found to be small, namely within their error limit.[62] For the Rydberg lifetime τ_R the D effect is normal, as expected for a motion along a pure twist via a nearly negligible barrier (see above). The D effect for the ground-state reactions was already discussed in section 4.2.3.

The ground-state processes, which we found, indicate that one of the time constants (τ_3) represents the lifetime of the carbene CH_3CH and the other (τ_4) that of hot ethylene, implying that both species are formed from the same S_1/S_0 CI (section 4.2.3). This means that the CI involves a partial H migration. More strictly speaking, the intersection-space region involving such a migration seems easily accessible for the wave packet (probably supported by an early acceleration into this direction near the V/Z CI, see above), although perhaps a region without it (but with twist and pyramidalization, for instance) might be competitive. An H-migration CI was already suggested by Evleth and Sevin and by Ohmine[29,30] and its importance pointed out once more by Freund and Klessinger,[26] although they predicted a less symmetric structure. Later calculations preferred the one-sided pyramidalization (after a 90° twist).[21,27,37−39] Recent high-level calculations point out the importance of H-migration for understanding hydrogen scrambling before dissociation.[20,35] However, they suggest that this CI (with imposed C_s symmetry) is not the minimum of the intersection space but a saddle point within it[20,35] (see also refs 27 and 31), whereas at a less high level and without symmetry constraint, the twisted-pyramidalized CI is at higher energy than the H-migration CI.[32] The result that releasing the C_s symmetry constraint lowers the H-migration CI was already obtained earlier.[26] The strong ethylidene signal in our experiment indicates that the H migration channel is at least competitive, perhaps even dominant. (It is remarkable in this context that the semiempirical dynamics calculation of Granucci et al.[33] used a low-energy H-migration CI and obtained a realistic S_1 lifetime, whereas the higher-level dynamics calculations, which did not have this CI or placed it at higher energy, obtained much longer lifetimes.[12,34−38]) But we suppose that the landscape of the S_1 potential in the region between the perpendicular minimum and the last CI is rather flat in several directions; this would explain why a momentum acquired in the Franck−Condon region can influence the photochemical outcome in olefins (section 4.2.6).

The general picture of a wave packet relaxing down along potential surfaces (Figures 6, 7, and 10) deserves additional comments. The wave packet is accelerated by the slopes, so that electronic energy is converted in this way to nuclear motion in this direction. Figures 7 and 10 suggest that on the way from the FC region (L_1) all excess energy is deposited in the twist coordinate and (as concluded above from the small deuterium effect) in part also to CC stretching. If no new coordinates were activated in L_2 to accept kinetic energy, the molecule would, also in L_2, keep performing hindered free rotation (with amplitudes $\varphi > 180°$) just as in the FC region. But the different isotope effect in L_2 indicates that the twist energy has dropped to some extent (amplitude $\varphi < 180°$; see sections 4.2.2 and 4.2.4). Obviously the cut in twist direction (Figures 6, 7, and 10) only provides an incomplete picture, even with taking CC stretching into account; there must be additional downslopes. Candidates may be the pyramidalization and CH bending (or beginning H migration), which we suggested to be initiated on entering L_2.

It should be noted that with the involvement of more coordinates, the wave packet does not become diffuse (which would prevent observation of coherent oscillations), and thus the process does not involve intramolecular vibrational energy redistribution (IVR) in the statistical sense; statistical IVR is only expected later, when the wave packet is reflected from slopes in other regions of the potential. The conversion of electronic to nuclear kinetic energy may be facilitated before and after the last CI, where there are slopes in a number of coordinate directions. But the energy distribution resulting immediately after passing the CI is still not necessarily statistical.

A final question is whether the measured times are not too short for the applicability of the Born−Oppenheimer approximation of separate time scales for electronic and nuclear motion, and thus for the possibility to draw potentials. Indeed, our times are shorter than the periods of some vibrations. (E.g., for a CC stretch around 1200 cm^{-1} or 0.15 eV the period would be 28 fs.) Nevertheless the electronic time scale is still much shorter, as to conclude from the energy difference between electronic states, which is several electronvolts, unless one is near a CI. In the latter region, electronic motion is slow, and this is just why the Born−Oppenheimer approximation breaks down and the wave packet can jump there to the lower surface.

4.2.6. Implications for Photochemistry. The fact that we observed a signal not only from hot ethylene (L_4) but also from ethylidene (L_3) after passing through L_2 implies that both species are formed from the same funnel, i.e., from the same region of the S_1/S_0 intersection space. Certainly also more generally the typical olefin reactions (cis−trans isomerization and carbene formation, besides internal conversion back to the reactant) originate and branch from the same CI or from a region nearby. Hence in the CI, H migration or an analogous alkyl-group migration has partially taken place (i.e., an H or alkyl bridge has formed), as pointed out above. This idea is also supported by the fact that it can explain several photochemical observations:

(1) In the condensed phase, reactions from the hot ground state are normally partially or completely suppressed, if the collisional cooling rate (typical time constant ≈10 ps, see, e.g., refs 97−99) is comparable to, or faster than, the reaction. H and H_2 elimination from *ethylene* have very similar activation energies (endothermicities) (see the energy diagrams in refs 52, 80, and 100) and should have similar rates. Nevertheless, the H channel is much more suppressed than H_2 elimination in condensed phase and even already in the gas by buffer gas.[41,101] This would not be understandable, if H_2 were formed from hot ethylene alone, even if this path can lead via ethylidene. However, if ethylidene is directly formed from the CI (i.e., not via ground-state ethylene), H_2 can form with very little activation energy (Figure 9), which implies much less temperature (and hence cooling-rate) sensitivity than via ethylene. The observation that H elimination is largely suppressed in the condensed phase also supports our assignment of a lifetime (τ_4) of several picoseconds to this dissociation; an assignment to a subpicosecond time (τ_3) would not be consistent with a suppression of this channel. Conversely, the survival of H_2 elimination in the condensed phase supports the assignment of the subpicosecond time (τ_3) to this process.

(2) Photolysis of liquid or solid ethylene also gives rise to methylcyclopropane, a typical product of a bimolecular reaction of a ground-state carbene (ethylidene) with the double bond of the olefin.[41,45] Already previously this product was taken as evidence for ethylidene formation from the CI.[45,47] Also the formation of butene-1 has been interpreted as a carbene insertion into the CH bond of ethylene.[45]

(3) On the one hand, cis−trans isomerization and carbene formation in the photolysis of ethylene and other olefins was already repeatedly suggested to take place from the same CI.[17,20,26,30,31,46,47,61,102,103] On the other hand, the yield ratio of carbene products to other reactions is larger, if alkylated olefins are irradiated at longer wavelengths, in the $\pi \rightarrow \sigma^*$ (or $\pi \rightarrow$ 3s Rydberg; the transition has a mixed character[2]) band preceding the $\pi \rightarrow \pi^*$ band in these compounds (reviews: refs 43 and 44 see also refs 40−42); branching in the Franck−Condon region

has been suggested in these cases.[43,44] However, we argue (section 4.2.5 and refs 102 and 103) that the Rydberg/$\pi\sigma^*$ and $\pi\pi^*$ states exchange population via a low-lying intersection of the potentials, and the wavelength dependence is to be interpreted by the wave packet momentum, which depends on the initial state.[102,103] Such a dynamical mechanism assumes that the momentum is conserved over a certain time and that the region of the CI is flat enough to permit an influence of the momentum on the branching. In ethylene itself, there is direct spectroscopic evidence that the π3s and $\pi\pi^*$ potentials cross at low energy, so that population can easily flow (within τ_R = 80 fs) from the former to the latter state, as discussed above (section 4.2.5).

We can also draw some conclusions from the short lifetimes that we measured:

The quantum yield of photodimerization of ethylene to cyclobutane is not measurable in the gas phase, and in liquid ethylene it is slightly below 10^{-3} (calculated from the relative yield of cyclobutane[101] and the quantum yield of H_2). This seems natural in view of the small τ_1 compared to a collision frequency. The latter is not well-defined in a condensed phase. But as a measure we can invoke one of the fastest collisional processes, cooling of the vibrational temperature, which has typical time constants around 10 ps (see, e.g., refs 97−99). Taking the ratio of our τ_1 and the 10 ps estimate of the collision time, one can expect just the quantum yield that has been found, if the reaction is very efficient in a close encounter. (In fact, if the two double bonds are fixed in one molecule in a short distance, such as in norbornadiene, the photochemical [2+2]-addition is ultrafast.[104]) Photodimerization is more efficient with other olefins[41,42] (see in particular the reviews in refs 105 and 106). In fact, they are likely to have longer excited-state lifetimes; some examples of longer lifetimes were found by Mestdagh et al. and by Hirayama and Lipsky:[61,107] Substitution by alkyl groups lowers the π3s Rydberg state (which also has $\pi\sigma^*$ character) to slightly below the $\pi\pi^*$ state, and population flows from the former to the latter (which is lowered along the twist coordinate) only via a small barrier (which is increased by lowering the Rydberg state)[102,103] and some olefins even fluoresce from the π3s/$\pi\sigma^*$ state, if the excess energy is not too high (e.g., tetramethylethylene[107−109]); a measurable fluorescence yield ($\approx 10^{-6}$) was even found from propylene,[107] whereas from ethylene it could never be detected. One can also expect that the excited-state lifetime is prolonged by delocalization, extending the π system by attaching a phenyl or a carboxyl group, for instance. In fact, good dimerization yields are obtained from such compounds.[105,106] Another effect that may enhance the dimerization yield is the direct excitation of van-der-Waals dimers (or molecule pairs fixed in another way, e.g., in a crystal[106]) to delocalized ("excimer") states, typically in the long-wavelength wing of the spectrum. In this case the molecule does not have to wait for a collision. An example is the photodimerization of cyclohexene;[102,110] the same mechanism was suggested for the dimerization of 7-dehydrocholesterol.[111]

Other bimolecular reactions are the expected addition reactions of polar reagents (e.g., methanol) to ethylene or other olefins in their zwitterionic excited state, which at 90° twist is nearly degenerate with the $\pi\pi^*$ state and can undergo sudden polarization.[17,22,23] The search for such reactions has not been very successful, and often it turned out that the addition products sometimes found were formed in the ground-state of a strained photoproduct such as the trans isomer of a cyclic olefin.[105,106] The reason is now clear: The perpendicular excited state is too short-lived (τ_2) to allow substantial yields of bimolecular reactions. To conclude from cyclohexene[102] and norbornene,[103] also in other simple olefins, the departure from S_1 through the last CI is barrierless and the time constant is also not substantially longer than in ethylene. With certain substituents (e.g., with several phenyl groups), however, the perpendicularly twisted form is stabilized and its lifetime can be much longer; in such cases, evidence for sudden polarization effects have indeed been found (see ref 24 and literature quoted therein).

Another bimolecular reaction is the addition of ethylidene (formed in its S_0 state from the CI) to ethylene. Its lifetime (τ_3) is also short. (To our knowledge it is the first time it has been measured directly and a spectroscopic signature of ethylidene was detected.) But it is ≈30 times longer than τ_1 or τ_2. In fact, in solid ethylene, methylcyclopropane and 1-butene (if this is also considered a carbene reaction product[45]) are formed in substantially higher yields than cyclobutane.[101] It was demonstrated that ethylidene (generated from another source) is long-lived enough to be trapped, for instance by reaction with CO in a cryogenic matrix,[112] although its direct detection by time-resolved spectroscopy failed due the (supposed and now determined) short lifetime.[113]

5. Conclusion

This work demonstrates that shortening the pulses (in particular the UV pump pulses) can reveal important new details in photochemical dynamics. Whereas previously, short time constants have been extracted from measurements with longer pulses by the help of deconvolution, it has only now been possible to nail down the small isotope effect on the lifetimes (an upper bound for it was found in ref 62), which in turn provides valuable information on the relaxation path and the potential. For resolving the coherent oscillations, short pulses are even indispensable; they cannot be extracted by deconvolution. For example, the 1570 cm^{-1} vibration with its 20 fs period requires a resolution around 10 fs. In the Franck−Condon region, the isotope effect on the torsion vibration (hindered free rotation) was found to be small; the vibration must therefore be strongly mixed with the CC stretch, similarly as the relaxation coordinate. In contrast, the vibration during departure from the S_1 state is a pure CC stretch, which can be rationalized by the fact that the amplitudes of hydrogen vibrations are much more limited than in the Franck−Condon region.

The vibrational structure in electronic transitions of ethylene has been studied for decades, with the aim to find out the excited-state potentials. Such data are also used to test ab initio calculations, which are being pushed to higher and higher levels and which in turn provide a better understanding of the potentials and dynamics. We provide for the first time a set of vibrational data for both, C_2H_4 and C_2D_4, in the Franck−Condon region and in the region before departure to the ground state. They may also serve to calibrate simulations of UV and other spectra, to find out more vibrations.

Our results suggest that the initial relaxation on the $\pi\pi^*$ (V) surface involves CC torsion as far as to 90° (within slightly more time than τ_1), but from the beginning intimately coupled with stretching of the CC bond, which initially expands and then contracts again. (At large torsion the V state probably equilibrates with the zwitterionic (Z) state. However, our probing method cannot distinguish the V and Z states.) During τ_2, already before a twist of φ = 90° is reached, the wave packet is gradually accelerated toward a new direction, which eventually (still within τ_2) leads to a conical intersection (CI) with the ground-state surface. This additional distortion (besides a twist of 90° and some CC stretching) involves not only pyramidal-

ization of a CH_2 group (according to theory) but also partial hydrogen migration. This conclusion was deduced from the observation of CH_3CH (ethylidene) as a primary product besides hot ethylene. (The assignment was inferred from the detection of *two* ground-state reactions (time constants τ_3 and τ_4), indicating that there are *two* primary products.) It is well-known that the slope directions near the last CI decide on the fate of the reaction path and the type and yield of products. We use the observation of products to conclude on the slope directions. In quantum chemistry the H-migration CI is still under debate.

Our data also support a scenario where the region extending from the perpendicular (D_{2d}) minimum to the last CI is energetically flat along the coordinates for H migration, pyramidalization and twist. This is how we explain that the photoproduct spectrum of olefins (carbene products compared to cis−trans and other isomerizations) can be influenced by an initial momentum, which in turn depends on the initially excited state (Rydberg or $\pi\pi^*$). Previously, the wavelength dependence of photochemistry (i.e., the violation of the Kasha rule) was interpreted by assuming a branching in the Franck−Condon region. In contrast, we point out that the Rydberg state delivers its population (within τ_R) to the $\pi\pi^*$ surface via a CI, which at least in ethylene is spectroscopically well-known and easily accessible.

We also discuss bimolecular reactions in view of the excited-state lifetimes that we found. The departure from the S_1 state (within $\tau_2 = 17$ fs in ethylene) seems to be generally very short (<100 fs) in simple olefins (section 4.2.6), so that bimolecular reactions have little chance. This explains why the search for chemical consequences of sudden polarization (in the S_1 minimum) was not overly successful. The same interpretation might be valid for dienes. For longer-chain polyenes, however, a different explanation must be invoked: Although their 2A states can be much longer-lived,[114] these states are covalent and have an only normal polarizability. In contrast, the photodimerization yield shows much more variation from olefin to olefin. It can start already in the Franck−Condon region; in particular, if the Rydberg state is below the $\pi\pi^*$ state (as is the rule with alkylated olefins), the lifetime of the initially excited state can be long. In addition, excimer states can contribute (section 4.2.6). Another bimolecular reaction is the carbene addition of ethylidene in its ground state to ethylene, for instance. The ethylidene lifetime ($\tau_3 = 0.6$ ps) is apparently long enough for a bimolecular reaction in liquid or solid ethylene.

Acknowledgment. This work was supported by the Deutsche Forschungsgemeinschaft (project FU 363/1) and the European Union's Human Potential Program under contract MRTN-CT-2003-505138 (XTRA). We thank W. Radloff for helpful comments.

References and Notes

(1) Wilkinson, P. G.; Mulliken, R. S. *J. Chem. Phys.* **1955**, *23*, 1895.
(2) Merer, A. J.; Mulliken, R. S. *Chem. Rev.* **1969**, *69*, 639.
(3) Robin, M. B. *Higher excited states of polyatomic molecules*; Academic Press: New York, 1975; Vol. 2.
(4) Robin, M. B. *Higher excited states of polyatomic molecules*; Academic Press: New York, 1985; Vol. 3.
(5) Mulliken, R. S. *J. Chem. Phys.* **1977**, *66*, 2448.
(6) Mulliken, R. S. *J. Chem. Phys.* **1979**, *71*, 556.
(7) McDiarmid, R.; Charney, E. *J. Chem. Phys.* **1967**, *47*, 1517.
(8) Foo, P. D.; Innes, K. K. *J. Chem. Phys.* **1974**, *60*, 4582.
(9) Sension, R. J.; Hudson, B. S. *J. Chem. Phys.* **1989**, *90*, 1377.
(10) Ziegler, L. D.; Hudson, B. S. *J. Chem. Phys.* **1983**, *79*, 1197.
(11) Ben-Nun, M.; Martínez, T. J. *J. Phys. Chem. A* **1999**, *103*, 10517.
(12) Viel, A.; Krawczyk, R. P.; Manthe, U.; Domcke, W. *J. Chem. Phys.* **2004**, *120*, 11000.
(13) Merer, A. J.; Mulliken, R. S. *J. Chem. Phys.* **1969**, *50*, 1026.
(14) Borelli, R.; Peluso, A. *J. Chem. Phys.* **2006**, *125*, 194308.
(15) Hazra, A.; Chang, H. H.; Nooijen, M. *J. Chem. Phys.* **2004**, *121*, 2125.
(16) Orkin, V. L.; Huie, R. E.; Kurylo, M. J. *J. Phys. Chem. A* **1997**, *101*, 9118.
(17) Klessinger, M.; Michl, J. *Excited states and photochemistry of organic molecules*; VCH: New York, 1995.
(18) Buenker, R. J.; Bonačić-Koutecký, V.; Pogliani, L. *J. Chem. Phys.* **1980**, *73*, 1836.
(19) Krawczyk, R. P.; Viel, A.; Manthe, U.; Domcke, W. *J. Chem. Phys.* **2003**, *119*, 1397.
(20) Barbatti, M.; Paier, J.; Lischka, H. *J. Chem. Phys.* **2004**, *121*, 11614.
(21) Molina, V.; Merchán, M.; Roos, B. O.; Malmqvist, P. A. *Phys. Chem. Chem. Phys.* **2000**, *2*, 2211.
(22) Bonačić-Koutecký, V.; Bruckmann, P.; Hiberty, P.; Koutecký, J.; Leforestier, C.; Salem, L. *Angew. Chem., Int. Ed.* **1975**, *14*, 575.
(23) Salem, L. *Science* **1976**, *191*, 822.
(24) Zijlstra, R. W. J.; Grozema, F. C.; Swart, M.; Feringa, B. L.; van Duijnen, P. T. *J. Phys. Chem. A* **2001**, *105*, 3583.
(25) Viel, A.; Krawczyk, R. P.; Manthe, U.; Domcke, W. *Angew. Chem., Int. Ed.* **2003**, *42*, 3434.
(26) Freund, L.; Klessinger, M. *Int. J. Quantum Chem.* **1998**, *70*, 1023.
(27) Ben-Nun, M.; Martínez, T. J. *Chem. Phys.* **2000**, *259*, 237.
(28) Ben-Nun, M.; Martínez, T. J. *Adv. Chem. Phys.* **2002**, *121*, 439.
(29) Evleth, E. M.; Sevin, A. *J. Am. Chem. Soc.* **1981**, *103*, 7414.
(30) Ohmine, I. *J. Chem. Phys.* **1985**, *83*, 2348.
(31) Wilsey, S.; Houk, K. N. *J. Am. Chem. Soc.* **2002**, *124*, 11182.
(32) Laino, T.; Passerone, D. *Chem. Phys. Lett.* **2004**, *389*, 1.
(33) Granucci, G.; Persico, M.; Toniolo, A. *J. Chem. Phys.* **2001**, *114*, 10608.
(34) Brill, M. R.; Gatti, F.; Lauvergnat, D.; Meyer, H. D. *Chem. Phys.* **2007**, *338*, 186.
(35) Barbatti, M.; Ruckenbauer, M.; Lischka, H. *J. Chem. Phys.* **2005**, *122*, 174307.
(36) Barbatti, M.; Granucci, G.; Persico, M.; Lischka, H. *Chem. Phys. Lett.* **2005**, *401*, 276.
(37) Ben-Nun, M.; Martínez, T. J. *Chem. Phys. Lett.* **1998**, *298*, 57.
(38) Ben-Nun, M.; Quenneville, J.; Martínez, T. J. *J. Phys. Chem. A* **2000**, *104*, 5161.
(39) Quenneville, J.; Ben-Nun, M.; Martínez, T. J. *J. Photochem. Photobiol. A* **2001**, *144*, 229.
(40) Steinmetz, M. G. Photochemistry with short UV light. In *Organic Photochemistry*; Padwa, A., Ed.; Marcel Dekker: New York, 1987; Vol. 8, p 67.
(41) Collin, G. J. *Adv. Photochem.* **1988**, *14*, 135.
(42) Adam, W.; Oppenländer, T. *Angew. Chem.* **1986**, *98*, 659.
(43) Kropp, P. J. Photorearrangement and fragmentation of alkenes. In *Handbook of Organic Photochemisty and Photobiology*; Horspool, W. M., Song, P.-S., Eds.; CRC Press: Boca Raton, FL, 1995; p 16.
(44) Kropp, P. J. Photorearrangement and fragmentation of alkenes. In *Handbook of organic photochemistry and photobiology*; Horspool, W. M., Lenci, F., Eds.; CRC Press: Boca Raton, FL, 2004; p 13.
(45) Tschuikoff-Roux, E.; McNesby, J. R.; Jackson, W. M.; Faris, J. L. *J. Phys. Chem.* **1967**, *71*, 1531.
(46) Klessinger, M. *Pure Appl. Chem.* **1997**, *69*, 773.
(47) Fuss, W.; Lochbrunner, S.; Müller, A. M.; Schikarski, T.; Schmid, W. E.; Trushin, S. A. *Chem. Phys.* **1998**, *232*, 161.
(48) Cromwell, E. F.; Stolow, A.; Vrakking, M. J. J.; Lee, Y. T. *J. Chem. Phys.* **1992**, *97*, 4029.
(49) Stolow, A.; Balko, B. A.; Cromwell, E. F.; Zhang, J.; Lee, Y. S. *J. Photochem. Photobiol. A* **1992**, *62*, 285.
(50) Balko, B. A.; Zhang, J.; Lee, Y. T. *J. Chem. Phys.* **1992**, *97*, 935.
(51) Lin, J. J.; Hwang, D. W.; Lee, Y. T.; Yang, X. *J. Chem. Phys.* **1998**, *109*, 2979.
(52) Chang, A. H. H.; Mebel, A. M.; Yang, X. M.; Lin, S. H.; Lee, Y. T. *J. Chem. Phys.* **1998**, *109*, 2748.
(53) Chang, A. H. H.; Hwang, D. W.; Yang, X. M.; Mebel, A. M.; Lin, S. H.; Lee, Y. T. *J. Chem. Phys.* **1999**, *110*, 10810.
(54) Lee, S. H.; Lee, Y. S.; Yang, X. *J. Chem. Phys.* **2004**, *120*, 10983.
(55) Lee, S. H.; Lee, Y. C.; Lee, Y. T. *J. Phys. Chem. A* **2006**, *110*, 2337.
(56) Lee, S. H.; Lee, Y. T. *Chem. Phys. Lett.* **2006**, *419*, 158.
(57) Satyapal, S.; Johnston, G. W.; Bersohn, R.; Oref, I. *J. Chem. Phys.* **1990**, *93*, 6398.
(58) Yao, L.; Mebel, A. M.; Lu, H. F.; Neusser, H. J.; Lin, S. H. *J. Phys. Chem. A* **2007**, *111*, 6722.
(59) Farmanara, P.; Steinkellner, O.; Wick, M. T.; Wittmann, M.; Korn, G.; Stert, V.; Radloff, W. *J. Chem. Phys.* **1999**, *111*, 6264.
(60) Farmanara, P.; Stert, V.; Radloff, W. *Chem. Phys. Lett.* **1998**, *288*, 518.
(61) Mestdagh, J. M.; Visticot, J. P.; Elhanine, M.; Soep, B. *J. Chem. Phys.* **2000**, *113*, 237.

(62) Stert, V.; Lippert, H.; Ritze, H. H.; Radloff, W. *Chem. Phys. Lett.* **2004**, *388*, 144.
(63) Fuss, W.; Schmid, W. E.; Trushin, S. A. *J. Chem. Phys.* **2000**, *112*, 8347.
(64) Trushin, S. A.; Panja, S.; Kosma, K.; Schmid, W. E.; Fuss, W. *Appl. Phys. B: Laser Opt.* **2005**, *80*, 399.
(65) Kosma, K.; Trushin, S. A.; Schmid, W. E.; Fuss, W. *Opt. Lett.* **2008**, *33*, 723.
(66) Trushin, S. A.; Kosma, K.; Fuss, W.; Schmid, W. E. *Opt. Lett.* **2007**, *32*, 2432.
(67) Trushin, S. A.; Fuss, W.; Kosma, K.; Schmid, W. E. *Appl. Phys. B: Laser Opt.* **2006**, *85*, 1.
(68) Yatsuhashi, T.; Trushin, S. A.; Fuss, W.; Rettig, W.; Schmid, W. E.; Zilberg, S. *Chem. Phys.* **2004**, *296*, 1.
(69) Trushin, S. A.; Kosma, K.; Fuss, W.; Schmid, W. E. *Chem. Phys.* **2008**, *347*, 309.
(70) Baum, P.; Lochbrunner, S.; Gallmann, L.; Steinmeyer, G.; Keller, U.; Riedle, E. *Appl. Phys. B: Laser Opt.* **2002**, *74*, S219.
(71) Rijkenberg, R. A.; Buma, W. J. *J. Phys. Chem. A* **2002**, *106*, 3727.
(72) Shimanouchi, T. Tables of molecular frequencies consolidated; NSRDS-NBS 39; NBS: Washington, DC, 1972; Vol. 1.
(73) Trushin, S. A.; Sorgues, S.; Fuss, W.; Schmid, W. E. *ChemPhysChem* **2004**, *5*, 1389.
(74) Sannen, C.; Raşeev, G.; Galloy, C.; Fauville, G.; Lorquet, J. C. *J. Chem. Phys.* **1981**, *74*, 2402.
(75) Oblinger, M.; Lorquet, A. J.; Lorquet, J. C. *Int. J. Mass Spectrom. Ion Processes* **1997**, *167*−*168*, 149.
(76) Costa, F. *Int. J. Quantum Chem.* **2006**, *106*, 2763.
(77) Modarelli, D. A.; Platz, M. S. *J. Am. Chem. Soc.* **1993**, *115*, 470.
(78) Raghavachari, K.; Frisch, M. J.; Pople, J. *Chem. Phys. Lett.* **1982**, *85*, 145.
(79) Evanseck, J. D.; Houk, K. N. *J. Am. Chem. Soc.* **1990**, *112*, 9148.
(80) Peña-Gallego, A.; Martínez-Nuñez, E.; Vázquez, S. A. *Chem. Phys. Lett.* **2002**, *353*, 418.
(81) Kim, M. H.; Leskiw, B. D.; Shen, L.; Suits, A. G. *J. Phys. Chem. A* **2007**, *111*, 7472.
(82) Stockbauer, R.; Inghram, M. G. *J. Chem. Phys.* **1975**, *62*, 4862.
(83) Kimura, K.; Katsumata, S.; Achiba, Y.; Yamazaki, T.; Iwata, S. *Handbook of HeI photoelectron spectra of fundamental organic molecules*; Japan Scientific Soc. Press: Tokyo, 1981.
(84) Miron, E.; Raz, B.; Jortner, J. *J. Chem. Phys.* **1972**, *56*, 5265.
(85) Dauber, P.; Brith, M.; Huler, E.; Warshel, A. *Chem. Phys.* **1975**, *7*, 108.
(86) Merer, A. J.; Watson, J. K. G. *J. Mol. Spectrosc.* **1973**, *47*, 499.
(87) Warshel, A. M.; Karplus, M. *Chem. Phys. Lett.* **1972**, *17*, 7.
(88) Mebel, A. M.; Chen, Y. T.; Lin, S. H. *Chem. Phys. Lett.* **1996**, *258*, 53.
(89) Mebel, A. M.; Hayashi, M.; Liang, K. K.; Lin, S. H. *J. Phys. Chem. A* **1999**, *103*, 10674.
(90) Petrongolo, C.; Buenker, R. J.; Peyerimhoff, S. D. *J. Chem. Phys.* **1982**, *76*, 3655.
(91) Petrongolo, C.; Buenker, R. J.; Peyerimhoff, S. D. *J. Chem. Phys.* **1983**, *78*, 7284.
(92) Williams, B. A.; Cool, T. A. *J. Chem. Phys.* **1991**, *94*, 6358.
(93) Mebel, A. M.; Hayashi, M.; Lin, S. H. *Chem. Phys. Lett.* **1997**, *274*, 281.
(94) Hayashi, M.; Mebel, A. M.; Liang, K. K.; Lin, S. H. *J. Chem. Phys.* **1998**, *108*, 2044.
(95) Fuss, W.; Schmid, W. E.; Trushin, S. A. *Chem. Phys. Lett.* **2001**, *342*, 91.
(96) Garavelli, M.; Page, C. S.; Celani, P.; Olivucci, M.; Schmid, W. E.; Trushin, S. A.; Fuss, W. *J. Phys. Chem. A* **2001**, *105*, 4458.
(97) Benzler, J.; Linkersdörfer, S.; Luther, K. *J. Chem. Phys.* **1997**, *106*, 4992.
(98) Hold, U.; Lenzer, T.; Luther, K.; Reihs, K.; Symonds, A. *Ber. Bunsen-Ges. Phys. Chem.* **1997**, *101*, 552.
(99) Hippler, H.; Luther, K.; Troe, J.; Wendelken, H. J. *J. Chem. Phys.* **1983**, *79*, 239.
(100) Lin, J. J.; Wang, C. C.; Lee, Y. T.; Yang, X. *J. Chem. Phys.* **2000**, *113*, 9668.
(101) Hirokami, S.; Cvetanović, R. J. *J. Phys. Chem.* **1974**, *78*, 1254.
(102) Fuss, W.; Schmid, W. E.; Trushin, S. A. *J. Am. Chem. Soc.* **2001**, *123*, 7101.
(103) Fuss, W.; Pushpa, K. K.; Schmid, W. E.; Trushin, S. A. *J. Phys. Chem. A* **2001**, *105*, 10640.
(104) Fuss, W.; Pushpa, K. K.; Schmid, W. E.; Trushin, S. A. *Photochem Photobiol. Sci.* **2002**, *1*, 60.
(105) Kaupp, G. [2+2]-cyclobutane synthesis (liquid phase). In *CRC handbook of organic photochemistry and photobiology*; Horspool, W. M., Song, P.-S., Eds.; CRC Press: Boca Raton, FL, 1995; Vol. 1, p 29.
(106) Kaupp, G. Cyclobutane synthesis in the solid state. In *CRC handbook of organic photochemistry and photobiology*; Horspool, W. M., Song, P.-S., Eds.; CRC Press: Boca Raton, FL, 1995; Vol. 1, p 50.
(107) Hirayama, F.; Lipsky, S. *J. Chem. Phys.* **1975**, *62*, 576.
(108) Siebrand, W.; Dedonder-Lardeux, C.; Jouvet, C. *Chem. Phys. Lett.* **1990**, *174*, 558.
(109) Wickramaaratchi, M. A.; Preses, J. M. *Chem. Phys. Lett.* **1985**,
(110) Kropp, P. J.; Snyder, J. J.; Rawlings, P. C.; Fravel, H. G. J. *J. Org. Chem.* **1980**, *45*, 4471.
(111) Fuss, W.; Höfer, T.; Hering, P.; Kompa, K. L.; Lochbrunner, S.; Schikarski, T.; Schmid, W. E. *J. Phys. Chem.* **1996**, *100*, 921.
(112) Seburg, R. A.; McMahon, R. J. *J. Am. Chem. Soc.* **1992**, *114*, 7183.
(113) Sander, W.; Bucher, G.; Wierlacher, S. *Chem. Rev.* **1993**, *93*, 1583.
(114) Fuss, W.; Haas, Y.; Zilberg, S. *Chem. Phys.* **2000**, *259*, 273.

JP803548C